

Durham Research Online

Deposited in DRO:

08 October 2020

Version of attached file:

Accepted Version

Peer-review status of attached file:

Peer-reviewed

Citation for published item:

Phillips, Thomas B. and Magee, Craig (2020) 'Structural controls on the location, geometry and longevity of an intraplate volcanic system : the Tuatara Volcanic Field, Great South Basin, New Zealand.', *Journal of the Geological Society.*, 177 (5). pp. 1039-1056.

Further information on publisher's website:

<https://doi.org/10.1144/jgs2020-050>

Publisher's copyright statement:

Phillips, Thomas B. Magee, Craig (2020). Structural controls on the location, geometry and longevity of an intraplate volcanic system: the Tuatara Volcanic Field, Great South Basin, New Zealand. *Journal of the Geological Society* 177(5): 1039-1056. <https://doi.org/10.1144/jgs2020-050> © Geological Society of London 2020.

Additional information:

Use policy

The full-text may be used and/or reproduced, and given to third parties in any format or medium, without prior permission or charge, for personal research or study, educational, or not-for-profit purposes provided that:

- a full bibliographic reference is made to the original source
- a [link](#) is made to the metadata record in DRO
- the full-text is not changed in any way

The full-text must not be sold in any format or medium without the formal permission of the copyright holders.

Please consult the [full DRO policy](#) for further details.

Structural controls on the location, geometry, and longevity of an intraplate volcanic system – The Tuatara Volcanic Field, Great South Basin, New Zealand

¹*Thomas B. Phillips & ²Craig Magee

¹*Department of Earth Sciences, Durham University, Science Labs, Elvet Hill, Durham, DH13LE*

²*Institute of Geophysics and Tectonics, School of Earth Science and Environment, University of Leeds, Leeds, LS2 9JT, UK*

*Corresponding Author – thomas.b.phillips@durham.ac.uk

Abstract

Intraplate volcanism is widely distributed across continents. Yet controls on the 3D geometry and longevity of individual volcanic systems remain poorly understood. Geophysical data provide insights into magma plumbing systems, but due to relatively low resolution, it is difficult to evaluate how magma transits highly heterogeneous continental interiors. We use borehole-constrained 2D seismic reflection data to characterise the 3D geometry of a volcanic field offshore New Zealand's South Island, termed the Tuatara Volcanic Field, and investigate its relationship with pre-existing structure. The ~270km² field is dominated by a dome-shaped lava edifice, surrounded and overlain by ~69 volcanoes and >70 sills emplaced over 40 Myr from the Late Cretaceous to Early Eocene (~85 Ma–45 Ma). The Tuatara Volcanic Field is located above a basement terrane boundary represented by the Livingstone Fault; the recently active Auckland Volcanic Field is similarly located along-strike on the North Island. We suggest the Livingstone Fault controlled the location of the Tuatara Volcanic Field by producing relief at the base lithosphere, thereby focussing lithosphere detachment over ~40 Myr,

and provided a pathway that facilitated magma ascent. We highlight how observations from ancient intraplate volcanic systems may inform our understanding of active intraplate volcanic systems, including the Auckland Volcanic Field.

1 Introduction

Intraplate volcanism encompasses igneous activity away from and unrelated to plate boundary processes (e.g. subduction and mid-ocean ridge spreading). Such intraplate volcanic systems develop in a variety of forms, from the construction of volcanic chains (e.g., Davies et al., 2015), through to large caldera forming eruptions (e.g., Timm et al., 2009) or the formation of volcanic fields comprising small, relatively short-lived volcanoes (e.g., Németh, 2010; Németh et al., 2003; Reynolds et al., 2018). These different styles of volcanic activity reflect the range of processes that drive, and influence the location and longevity of, intraplate volcanism. For example, hotspot intraplate volcanism occurs above a fixed, thermal mantle anomaly, producing chains of extinct volcanoes as plate motion carries active volcanoes away from the melt source (e.g., Clague and Jarrard, 1973; Morgan, 1972; Sleep, 1992). In contrast, during continental rifting, the location and longevity of intraplate volcanic systems relates to the location and magnitude of lithospheric thinning (e.g., Wilson et al., 1995; Wu et al., 2018). In other intraplate settings, such as the Turkish-Iranian Plateau, Eastern Australia, or Zealandia, diffuse volcanism occurs seemingly randomly over wide (continental-scale) areas (e.g., Finn et al., 2005; Hoernle et al., 2006; Kaislaniemi et al., 2014; Rawlinson et al., 2017). Whilst records of intraplate volcanism across these broad areas may be relatively continuous, individual volcanic systems are typically active across much shorter (Myr) timescales. Relative to hotspot- or rift-related intraplate volcanism, the processes driving the formation of these diffuse volcanic fields are often elusive and we particularly poorly understand the factors controlling the distribution and longevity of individual volcanic systems (e.g. Valentine and Hirano, 2010). In the absence of a clear process-driven control on the distribution of intraplate volcanic fields, pre-existing lithospheric and/or crustal structures may represent a crucial and commonly overlooked influence on their siting, magma plumbing system structure, and longevity.

Constraining the 3D geometry of magma plumbing systems and assessing how intraplate volcanism relates to and/or may be influenced by pre-existing structures is difficult because (see Magee et al., 2018 and references therein): (i) geophysical and geodetic data typically provide only a relatively low resolution view of subsurface magma or igneous rock distribution, and capture little information on host rock structure; (ii) outcrop analyses of ancient plumbing systems allow detailed analyses of intrusion geometry and host rock structure, but limitations in exposure at Earth's surface mean we cannot often place these observations within a 3D context; and (iii) petrological and chemical data, whilst providing crucial insights into melt and magma evolution, are often interpreted within a poorly defined structural framework. Reflection seismology provides a powerful tool for imaging the 3D geometry of volcanoes and magma plumbing systems in the subsurface (e.g., Bischoff et al., 2017; Bischoff et al., preprint; Buntin et al., 2019; Magee et al., 2019; Magee et al., 2016; McLean et al., 2017; Morley, 2018; Quirie et al., 2019; Reynolds et al., 2017; Sun et al., 2019a).

Here, we use borehole-constrained seismic reflection data to investigate the 3D structure of an intraplate volcanic field buried within the Great South Basin, offshore of the South Island of New Zealand. The volcanic field comprises a ~270 km² central edifice, formed of stacked lavas, surrounded and overlain by at least 69 volcanic cones developed at varying stratigraphic levels; we also identify a network of >70 igneous sills that formed the shallow-level plumbing system and linked to individual volcanoes. We refer to this province as the 'Tuatara Volcanic Field' after the endemic New Zealand reptile, the name of which is derived from the Māori language and fittingly means 'peaks on the back'. The well exposed and studied basement geology onshore New Zealand (e.g., Mortimer, 2004; Tarling et al., 2019), combined with a detailed and comprehensive record of intraplate volcanism throughout the Cenozoic (e.g., Adams, 1983; Bischoff et al., preprint; Cooper et al., 1987; Hoernle et al., 2006; Németh and White, 2003; Rout et al., 1993; Speight, 1943; Stipp and McDougall, 1968; Waight et al., 1998) and high-resolution marine geological and geophysical data available in the offshore domain (e.g., Mortimer et al., 2002; Phillips and McCaffrey, 2019; Tulloch et al., 2019; Uruski, 2015; Uruski et al., 2007), allow us to fully characterise and constrain the internal architecture of the Tuatara Volcanic Field and assess how it relates to the surrounding crustal

structure. By identifying seismic-stratigraphic onlap and downlap relationships, we show the volcanoes and sills were emplaced between ~85 and ~45 Ma, recording ~40 Myr of punctuated igneous activity spanning the Late Cretaceous-to-Early Eocene.

We propose the location and longevity of the Tuatara Volcanic Field was controlled by the underlying terrane boundary marked by the Livingstone Fault. In particular, we suggest changing relief of the lithosphere-asthenosphere boundary across the terrane boundary promoted local lithospheric detachment and melting, whilst the Livingstone Fault facilitated magma ascent. The structural setting of the Tuatara Volcanic Field is equivalent to that of the recently active Auckland Volcanic Field on the North Island (active 193 Ka - 500 y BP; Hopkins et al., 2020; Lindsay et al., 2011). Our study of the Tuatara Volcanic Field, which highlights how pre-existing structure and sill-complex development can influence the location and longevity of volcanic activity, may offer important insights into the processes occurring at the Auckland Volcanic Field and intraplate volcanism elsewhere.

2 Geological setting

Zealandia is an ideal natural laboratory to explore how crustal structure may affect the distribution, geometry, and evolution of volcanic fields: it hosts a long record of intraplate volcanism, from the Cenozoic to present day, dispersed across the length and breadth of a continent comprising a heterogeneous basement formed of multiple distinct terranes (e.g., Mortimer, 2004; Mortimer et al., 2002; Mortimer et al., 1999; Phillips and McCaffrey, 2019; Tulloch et al., 2019). This study focusses on a ~10,000 km² area in the northern part of the Great South Basin, offshore the east coast of the South Island of New Zealand and located 60 km SE of the Dunedin Volcano on the Otago Peninsula (Figure 1). The study area forms part of the Campbell Plateau on the continental shelf of Zealandia, an extensive area of submerged and extended continental crust characterised by water depths of ~500–1500 m (Adams, 1962).

2.1 Regional geological evolution

The basement geology of New Zealand comprises the Austral Superprovince, which incorporates a series of terranes that accreted along the southern margin of Gondwana between the Cambrian-to-Cretaceous (e.g., Bishop et al., 1985; Howell, 1980; Johnston, 2019; Mortimer, 2004; Mortimer et al., 2014). These terranes are divided into the Eastern and Western provinces, which are separated by the Median Batholith (Figure 1) (Mortimer, 2004; Mortimer et al., 1999). Projecting onshore terrane boundaries offshore along-strike suggests the study area resides within the Eastern Province and spans the faulted boundary between the Caples Terrane and the Dun Mountain-Maitai Terrane (Figure 1). This terrane boundary corresponds to the Livingstone Fault (Figure 1), which is a serpentinite-dominated shear zone that ranges from 10's to 100's of metres wide, dips steeply to the northeast, and extends down to, at least, the base of the crust (Mortimer et al., 2002; Tarling et al., 2019). The Caples Terrane comprises weakly metamorphosed volcanoclastic greywackes, which accreted to the southern margin of Gondwana during the Permian-to-Triassic (Johnston, 2019; Mortimer, 2004; Robertson et al., 2019), whilst the Dun Mountain-Maitai Terrane includes the Early Permian Dun Mountain, mafic-to-ultramafic ophiolite belt and an overlying, 6 km thick sequence of Late Permian-Middle Triassic volcanoclastic sedimentary rocks (i.e. the Maitai Group; Mortimer, 2004). Due to its mafic/ultramafic lithology, the Dun Mountain ophiolite is delineated by the Junction Magnetic Anomaly, which forms a ~20 km wide positive anomaly onshore (e.g., Davey and Christoffel, 1978; Sutherland, 1999; Tulloch et al., 2019), but is less prominent offshore (Figure 2). Further positive magnetic anomalies, forming part of the Stokes Magnetic Anomaly System, are identified south of the Junction Magnetic Anomaly and likely relate to the Rotorua igneous province and additional volcanics within the Eastern Province terranes (Figure 2) (Grobys et al., 2009; Hunt, 1978; Sutherland, 1999; Woodward and Hatherton, 1975).

Subduction and terrane accretion along the southern margin of Gondwana ceased during the mid-to-late Cretaceous as the Hikurangi Plateau, part of a Large Igneous Province, collided with and jammed the subduction zone (Davy et al., 2008). Following the cessation of subduction, Zealandia underwent two major phases of rifting related to the breakup of Gondwana during the Late Cretaceous (Figure 1B) (Kula et al., 2007; Laird and Bradshaw, 2004; Mortimer et al., 2019; Tulloch et al., 2019; Uruski

et al., 2007). Initial rifting from ~100–90 Ma related to break-up between Zealandia and Australia, and may have led to extensional reactivation of terrane boundaries beneath the proto-Great South Basin (Figure 1) (Phillips and McCaffrey, 2019). The second rift phase occurred from ~90–80 Ma in response to extension between Zealandia and Western Antarctica, resulting in the formation of the NE-trending Great South and Canterbury basins (Figure 1) (Beggs, 1993; Grobys et al., 2009; Kula et al., 2007; Tulloch et al., 2019).

The Alpine Fault formed during the Early Cenozoic to accommodate plate motion between the Pacific and Australian plates. Although located relatively close (~200 km) to the Alpine Fault between the Pacific and Australian plates, the Great South and Canterbury basins were relatively tectonically stable, and not influenced by back-arc extension or Alpine deformation, following Late Cretaceous rifting. The Alpine Fault offset the basement terranes across Zealandia, such that those beneath the South Island are also present beneath parts of the North Island (e.g. Cassidy and Locke, 2010; Collanega et al., 2018; Cooper and Norris, 1994; Howell, 1980; Lamb et al., 2016; Muir et al., 2000; Tarling et al., 2019). In particular, the Dun Mountain-Maitai and Caples terranes, which underlie our study area, are present beneath the Auckland Volcanic Field in the North Island (Figure 1) (Cassidy and Locke, 2010; Hopkins et al., 2020; Le Corvec et al., 2013; McGee et al., 2013; Spörli et al., 2015).

Late Cretaceous syn-rift strata within the Great South Basin, which were deposited unconformably onto the Permian-to-Triassic crystalline basement of the Caples and Dun Mountain-Maitai terranes, are dominated by siliciclastic rocks and coal measures of the Hoiho Group (Figure 1b) (Higgs et al., 2019; Killops et al., 1997; Sahoo et al., 2014). Widespread deposition of deep marine mudstones and siltstones occurred across the majority of the Great South and Canterbury Basins during the Cenozoic, with some carbonate deposition in the Oligocene-Miocene (Fig. 1b) (Bertoni et al., 2019; Chenrai and Huuse, 2020; Morley et al., 2017). The Marshall Paraconformity forms the Oligocene-Eocene boundary across the area and is purported to be related to the onset of the Antarctic circumpolar current (Fulthorpe et al., 1996; Morley et al., 2017). Much of the shallow stratigraphy across the Great South and Canterbury Basins has been reworked into contourite deposits (Figure 1b) (Fulthorpe et al.,

1996; Lu and Fulthorpe, 2004). At the present day, a series of steep-sided canyons traverse the seabed across the area, often eroding down to the Marshall Paraconformity surface (Figure 1b).

2.2 Intraplate igneous activity across Zealandia

Following the breakup of Gondwana in the Late Cretaceous, widespread and long-lived magmatic and volcanic activity has occurred in intraplate settings across Zealandia. Aside from back-arc rifting and associated volcanism in the Taupo Volcanic Zone (1.5 Ma–Present), examples of Late Cretaceous and/or Cenozoic intraplate volcanic systems include: the Auckland Volcanic Field (193 Ka – 500 y BP) on the North Island (Acocella et al., 2003; Cassidy and Locke, 2010; Hopkins et al., 2020; Le Corvec et al., 2013; McGee et al., 2013); and the Akaroa and Lyttleton volcanoes (12–6 Ma), and the Dunedin Volcano (16–11.7 Ma) of the Banks and Otago Peninsulas, respectively, on the South Island (Figure 1) (Price and Chappell, 1975; Speight, 1943; Stipp and McDougall, 1968). Offshore New Zealand, the Auckland (~37–19, 25–12 Ma) and Chatham islands (85–82, 41–35, 6–3 Ma) located towards the eastern and southern margins of Zealandia, respectively, were also repeatedly active during the Late Cretaceous-to-Cenozoic (Adams, 1983; Grindley et al., 1977), with further magmatic and volcanic activity having been documented in the Canterbury and Taranaki basins during the Miocene (Bischoff et al., preprint; Bischoff et al., 2017; Morley, 2018; Reeves et al., 2018). A detailed catalogue of the timings of intraplate volcanism across Zealandia can be found in Hoernle et al. (2006) and Timm et al. (2010), and references therein, with further examples of intraplate volcanism shown in Figure 1a.

The causal mechanism for the diffuse Cenozoic-to-present record of intraplate volcanic activity across Zealandia is difficult to reconcile with fixed hotspot- and rift-related processes (Timm et al., 2010). For example, volcanic activity is not compatible with a plume-related origin as such a long record of activity would require a static Zealandia relative to a ‘fixed’ mantle source; yet plate motion data indicate Zealandia has moved ~4000 km N/NW during the Cenozoic (Clouard and Bonneville, 2005; Hoernle et al., 2006; Sutherland, 1995; Wright et al., 2016). Furthermore, aside from igneous activity

related to back-arc rifting in the Taupo Volcanic Zone, Cenozoic magmatism across Zealandia is not related to lithospheric thinning and extension, which ceased during the Late Cretaceous (Figure 1b) (Acocella et al., 2003; Kula et al., 2007; Laird and Bradshaw, 2004; Mortimer et al., 2019). The igneous rocks sampled onshore New Zealand also show an OIB-type affinity not compatible with rift-related magmatism; their composition, including silica-undersaturated nephelenites and basanites, suggests they were derived from an asthenospheric source with varying degrees of input from a metasomatised mantle lithosphere (Finn et al., 2005; Hoernle et al., 2006). Intraplate volcanism across Zealandia is instead proposed to relate to localised detachment of dense material from the base of the lithosphere, small-scale convection, and decompression melting of upwelling asthenosphere (Elkins-Tanton, 2005; Hoernle et al., 2006; Timm et al., 2009; Timm et al., 2010). As a driver for lithosphere detachment, it has been suggested that the lithosphere beneath Zealandia contains large amounts of garnet pyroxenites and eclogites following protracted subduction, creating a contrast between dense lower lithosphere and relatively less dense upper asthenosphere (Elkins-Tanton, 2005; Hoernle et al., 2006; Timm et al., 2009). Similarly, increased mantle water content in a post-subduction setting may decrease mantle viscosity and lower the peridotite solidus, resulting in small-scale convection at the base of the lithosphere (Elkins-Tanton, 2005; Kaislaniemi et al., 2014). A key component of this coupled lithosphere detachment and small-scale convection mechanism is that the magma source is not fixed in specific locations in the mantle or lithosphere, allowing individual intraplate volcanic systems to occur over widespread areas and long timescales.

3 Data and methods

3.1 Available data and seismic interpretation

In this study, we use 2D seismic reflection data from three different surveys (OMV, DUN and HUN), with a total line length of >50,000 km. These datasets were acquired over a range of years (1972, 2006, and 2008) and, accordingly, have different acquisition and processing parameters. Two of the surveys (OMV, DUN) record to ~8 s two-way travel-time (TWT), whilst the HUN survey records to ~5 s TWT. Seismic lines are typically oriented either NE-SW or NW-SE, and have a maximum

spacing of 2 km in the NE direction and ~8 km in the NW direction (Figure 2). All seismic data are zero phase and displayed in normal polarity, such that a downward increase in acoustic impedance (e.g., the seabed) is represented by a peak (red) reflection, with a downward decrease in acoustic impedance represented by a trough (blue). The seabed across the study area is cut by multiple, steep-sided, up to ~0.5 s TWT deep canyons, which often produce geophysical artefacts (multiples) at deeper stratigraphic levels that partially obscure reflection configurations. There are no boreholes in the study area but we tie our seismic data to the Toroa-1 well, located ~140 km to the SW, to constrain ages of key stratigraphic units (Figure 1a). The magnetic data used in this study are shown as reduced to pole in order to place the anomalies vertically above the magnetic source (Figure 2).

3.2 Seismic resolution

The limit of separability (wavelength (λ)/4) within the sedimentary succession of interest, based on an average seismic velocity of ~3 km s⁻¹ for the stratigraphic sequence derived from the Toroa-1 borehole (Figure 1) and an average dominant frequency of ~30 Hz, is ~25 m; the limit of visibility ($\lambda/30$), i.e. the thinnest structure that will be detected in the data, is ~3 m (Slatt, 2006). Features imaged in the seismic data that are thicker than the limit of separability will produce discrete reflections that can be linked to their top and base, whilst features with a thickness between the limits of separability and visibility will be displayed as tuned seismic reflection packages (Kallweit and Wood, 1982; Widess, 1973). Such tuned reflection packages occur because reflections from the top and base of the same feature interfere on their return to the surface and cannot be deconvolved (Brown, 2011).

No igneous features associated with the Tuatara Volcanic Field are penetrated by boreholes, so we do not know their composition or seismic velocity. However, based on comparison to the Maahunui Volcanic Field located in the northern Canterbury Basin, where the Resolution-1 boreholes intersect a gabbroic sill (Bischoff et al., 2020; Bischoff et al., 2019; Magee et al., 2019), and to volcanic fields sampled onshore New Zealand (Hoernle et al., 2006; Németh and White, 2003; Timm et al., 2009), we infer the Tuatara Volcanic Field is likely dominantly mafic. From an average interval velocity of ~5.2 km s⁻¹ for the gabbroic sill intersected by Resolution-1 (Magee et al., 2019), coupled with

estimated velocity ranges for mafic volcanic fields imaged in seismic reflection data elsewhere (e.g., western India - $\sim 3.3\text{--}5.5\text{ km s}^{-1}$, Calvès et al. (2011); Australia, Bight Basin - $\sim 2.4\text{--}6.7\text{ km s}^{-1}$, Magee et al. (2013b); Australia, Bass Basin - $2.2\text{--}4.0\text{ km s}^{-1}$, Reynolds et al. (2018)), we anticipate that igneous rocks within the Tuatara Volcanic Field likely have an average seismic velocity of $4.5 \pm 1.5\text{ km s}^{-1}$. Combined with a dominant seismic frequency of $\sim 30\text{ Hz}$ within the depth interval of the Tuatara Volcanic Field, our inferred velocities correspond to limits of separability and visibility of $\sim 25\text{--}50\text{ m}$ and $3\text{--}7\text{ m}$, respectively. As we do not know the detailed velocity structure of the volcanic province and surrounding strata, particularly its lateral variability, we do not depth-convert the seismic reflection data and present measurements in time rather than depth to avoid additional errors.

3.3 Interpreting and dating volcano-magmatic features

We identify and map a series of different igneous sills, lavas, and volcanoes across the study area based on their (e.g. Eide et al., 2018; Planke et al., 2005; Planke et al., 2000; Symonds et al., 1998; Thomson, 2005): (i) relatively high amplitude compared to stratigraphic reflections; (ii) positive polarity; (iii) limited lateral extent; and (iv) geometrical similarity to sills, lavas, and volcanoes observed elsewhere. Sills were also mapped based on whether their corresponding reflection cross-cuts, but does not offset background stratigraphic reflections (e.g. Magee et al., 2016; Planke et al., 2005; Thomson and Hutton, 2004). To constrain the relative age of inferred volcano-magmatic features, we mapped five stratigraphic horizons across the area that we correlated to the Tara-1 and Toroa-1 wells located $\sim 130\text{--}140\text{ km}$ to the south (Figure 1 and Supplementary Figure 1): Top Coniacian ($\sim 86.3\text{ Ma}$); Top Cretaceous ($\sim 66\text{ Ma}$); Top Paleocene ($\sim 56\text{ Ma}$); Top Early Eocene ($\sim 45.7\text{ Ma}$); and the Marshall Paraconformity (Base Oligocene $\sim 33.9\text{ Ma}$). There is no well control on deeper stratigraphic levels throughout the Great South Basin, although a tentative top crystalline basement, corresponding to a high-amplitude reflection separating overlying continuous reflections from underlying chaotic reflectivity, is interpreted on individual sections (Sahoo et al., 2014; Uruski et al., 2007; Uruski, 2010). From these mapped stratigraphic horizons, we can constrain the relative timing of emplacement of different igneous features by: (i) determining the age interval of strata that interpreted volcanoes and lavas were erupted onto (i.e. the syn-volcanic palaeosurface), and the age

interval of strata that directly overlies and onlaps onto them (e.g. Magee et al., 2013b; Symonds et al., 1998); (ii) dating strata encasing sills, which the intrusions must post-date; and (iii) defining the age of strata onlapping onto intrusion-induced forced folds above sills, where observed, which formed at the contemporaneous free surface to accommodate sill intrusion (Hansen and Cartwright, 2006; Magee et al., 2017; Reeves et al., 2018; Trude et al., 2003).

As only 2D seismic reflection data are available, many volcano-magmatic features are only observed on individual 2D lines, meaning we cannot assess or quantify their individual 3D geometry. Where volcano-magmatic features can confidently be mapped across several 2D lines, we utilise the seismic software to interpolate our 2D horizon interpretations and recover their approximated 3D structure (see Hansen et al., 2008). Whilst this interpolation technique is broadly applied to extract information on the 3D geometry of volcanoes and sills imaged in 2D seismic reflection, the 2D seismic lines may not intersect the centre or maximum diameter of any specific feature (e.g., Hansen et al. 2008; Magee et al. 2013). Furthermore, we acknowledge that seemingly isolated features interpreted on different sections may in fact form part of a larger, singular structure. Quantitative measurements can therefore only be considered to represent minimum estimates. Finally, we note that some small volcano-magmatic features present in the study area may occur between and thus not be imaged by our 2D seismic grid.

4 Identification of volcano-magmatic structures in the Tuatara

Volcanic Field

We recognise a variety of different intrusive and extrusive igneous features that we can differentiate based on their location relative a central structural high, which we term the ‘Central edifice’. For clarity, here we sequentially describe and interpret the origin and age of: (i) high-amplitude reflectivity comprising the Central edifice; (ii) mound-like structures atop and beyond the lateral

limits of the Central edifice; and (iii) intrusive features, and associated host rock structures, beyond the lateral limits of the main edifice.

4.1 Central edifice

4.1.1 Observations

The Tuatara Volcanic Field is characterised by a ~0.5 s TWT thick package of stacked, broadly sub-parallel, high-amplitude seismic reflectivity that thins towards its margins and forms a convex-upwards domal structure (Figures 2, 3, 4); we term this the Central edifice. The top of the reflection package has a positive polarity, indicating it corresponds to a downwards increase in acoustic impedance (e.g., Figs 3, 4). Beneath this high-amplitude reflection package, seismic reflections appear dimmer and more chaotic (i.e. they are ‘washed out’) compared to areas at the same structural level beyond the lateral limits of the Central edifice (Figs 3, 4). Despite the poorer imaging beneath the high-amplitude reflection package, we are able to tentatively map the underlying top acoustic basement and, occasionally, the Top Coniacian and Top Cretaceous horizons (Figs 3, 4); we note that the most prominent reflections often correspond to seafloor canyon-related multiples (Fig. 3). Some offset reflections across potential faults can also be tentatively identified on individual seismic sections (Figure 3).

In plan-view, the high-amplitude reflection package defining the Central edifice displays an elliptical geometry, covering ~270 km², with a NW-trending long axis 23 km in length and a 15 km long, NE-trending short axis (Figure 2b). The upper surface of the high-amplitude reflection package reaches 2 s TWT at its shallowest point in the centre and deepens to 2.5–3 s TWT around its margins (Figures 2b, 3, 4). At the deepest part of its upper surface, Upper Cretaceous strata onlap onto the high-amplitude reflection package (Figure 3), whilst at shallower depths it is onlapped and overlain by Early Eocene strata. In places, the top Paleocene horizon can be mapped through the upper portion of the high-amplitude reflection package (Figure 3, 4).

We also identify some areas of lower amplitude reflectivity within the reflection package, which typically correspond to mound-shaped features (see section 4.2), or reflections displaying a clinoform-like geometry (Figs 3, 4); i.e. they consist of gently dipping reflections with a sigmoidal geometry <100 ms TWT high. The top inflexion point of these sigmoidal reflections is typically horizontal across the reflection package (Figure 5).

4.1.2 Interpretation

We interpret the domal package of high-amplitude reflectivity as a series of stacked, tabular lava sequences based on: i) the high-amplitude and positive polarity of the reflections, consistent with a downwards increase in acoustic impedance from lower velocity ($\sim 3 \text{ km s}^{-1}$), lower density sedimentary rocks above into higher velocity ($\sim 4.5 \text{ km s}^{-1}$), higher density igneous lavas; ii) the inference that underlying reflections locally display a convex-upwards morphology, which could be a geophysical velocity ‘pull-up’ artefact akin to those observed beneath volcanoes elsewhere and related to seismic energy travelling through an overlying high velocity layer (e.g. Magee et al., 2013b; Sun et al., 2019a); iii) the lack of reflectivity beneath the package, as high impedance lavas can scatter and attenuate seismic energy, restricting imaging of underlying layers (e.g. Gallagher and Dromgoole, 2007; Maresh et al., 2006); and iv) the laterally discontinuous nature of the reflections, forming an isolated domal structure, suggestive of a non-sedimentary origin (Figure 3, 4). Similarities between the seismic expression of tabular lava sequences identified and confirmed by boreholes elsewhere and the domal high-amplitude reflection package we observed, supports our interpretation that the Central edifice comprises a stacked lava sequence (McLean et al., 2017; Quirie et al., 2019; Walker et al., 2019). Our tentative interpretation that normal faults can be recognised beneath the high-amplitude reflection package suggests that the edifice was erupted atop a horst-like structure formed during earlier rifting; this inference remains contentious as we are unable to correlate interpreted faults across multiple seismic sections and thus cannot confirm the basement structure (Figure 3, 4). We suggest this pre-existing horst-like structure likely formed a partly buried, structural high during volcanism, with extrusion preferentially occurring towards its top surface, where the lavas are thickest (Figure 3, 4).

Based on their location within and associated with the stacked lava sequences, we suggest the relatively low-amplitude, sigmoidal reflection packages may also be igneous in origin. In particular, we consider these sigmoidal reflection packages correspond to lava or hyaloclastite deltas, as they appear similar in their geometry, structural setting, and seismic character to examples identified, and occasionally drilled, in other sedimentary basins (Planke et al., 2000; Wright et al., 2012). Using the sequence-stratigraphic terminology applied to clinoforms, the sigmoidal reflection packages described here represent dominantly progradational sequences, indicative of transport away from areas of higher relief, with little to no aggradation (Figure 5). The relatively small height (<100 ms TWT) and progradational character of these sequences suggests that they built outwards into a shallow water environment of similar depth to the clinoform height (~100-150 m) (Figure 1b) (Patruno and Helland-Hansen, 2018; Wright et al., 2012). The presence of potential lava and/or hyaloclastite deltas, coupled with its domal geometry, suggest the Central edifice of the Tuatara Volcanic Field may have formed a shallow-water bathymetric high during its formation (Figure 3).

At its deepest, the base of the Central edifice lava sequence occurs within Upper Cretaceous strata (i.e. extending just below the Top Coniacian), which also onlaps onto the lowermost section of the top lava sequence (Figure 3); these observations suggest lava extrusion to form the Central edifice initiated in the Upper Cretaceous, perhaps towards the end of the Coniacian (~86 Ma). It is difficult to determine whether the edifice was constructed during a single event or through multiple, periodic extrusive phases because we cannot distinguish whether the overlapping Palaeocene and Early Eocene strata was deposited around a pre-existing dome or on a progressively growing structure. However, on some 2D seismic lines, interpreted stratigraphic horizons can seemingly be mapped into the stacked lavas sequences, and thus potentially represent syn-volcanic paleosurfaces that allow us to constrain edifice growth (Figure 3, 4). The interpreted top basement horizon continues beneath and thus predates the formation of the Central edifice (Figure 4). Whilst the top Coniacian horizon also appears to mostly continue beneath the Central edifice (Figure 4), in some areas it extends into the highly reflective lava sequences, suggesting that this interval corresponds to an early stage of Central edifice construction (Figure 3). At shallow depths, the top Early Eocene horizon blankets the edifice

indicating that it postdates its formation. Between these maximum and minimum age constraints, the top Paleocene horizon appears to represent the basal surface of a lava sequence in the upper parts of the high-amplitude reflection package (Figure 4), suggesting the Central edifice formed through at least two extrusive events in the Upper Cretaceous and towards the end Palaeocene.

4.2 Mound-shaped features

4.2.1 Observations

We identify a total of 69 mound-shaped features distributed atop, within, and around the Central edifice at multiple stratigraphic levels spanning the Cretaceous-to-Early Eocene (Figure 2b, 6). These mound-shaped features are characterised by a variable amplitude, typically positive polarity top surface and a sub-horizontal, conformable basal reflection (Fig. 6). Where reflections are resolved within the mounds, they are typically low- to moderate-amplitude and either parallel the top mound surface or appear sub-horizontal (Figure 5b). The majority of mounds have a prominent peak (Figure 6b, e, f), although some display a flatter top (Figure 6a, c). The mounds typically have minimum heights of ~25 ms TWT and basal diameters of ~1–2 km, with the largest reaching minimum heights of up to 400 ms TWT and basal diameters of ~3 km (Figure 6).

The mounds are located proximal to the Central edifice, with the majority (~43) situated atop or within the high amplitude reflection package (Figure 3, 4, 7a). The top of the edifice is characterised by two large conical features surrounded by stacked lava sequences (Figure 2b, 6a). Further mounds are identified at different stratigraphic levels within the edifice itself (Figure 3, 6a). In some instances we observe that the high-amplitude reflections interpreted as lavas are often spatially related to the mounds identified here, being located around their margins and often draping atop the structures (Figure 6a, e).

Reflections immediately overlying the basal surface of the mound-shaped features onlap onto the flanks of the mound tops (Figure 6). Above the mound summits, reflections appear to deflect upwards, forming anticlinal folds, which occasionally host crestal faults; no reflections onlap these supra-mound folds but we note fold amplitude decays upwards (Figure 6a, d). Within one of these

supra-mound folds, a bright, high-amplitude, and horizontal reflection cross-cuts the folded strata (Figure 6e). In some instances, the mounds are associated with underlying vertical zones of seismic disturbance characterised relatively low-amplitudes and reflection deflection (e.g., Figure 6f).

To the south of the Central edifice, we identify multiple high-amplitude, positive polarity, tuned reflection packages within the Lower Eocene succession (Figure 2a, 4, 8). These high-amplitude reflections are situated beneath, but close to, the top Early Eocene horizon and are downlapped by Early Eocene-aged strata (Figure 2, 8). In places, the high-amplitude reflections appear to cross-cut and/or truncate underlying reflections (Figure 8). The amplitude of these high-amplitude reflections decreases towards a small (~300 m wide), 60 ms TWT high mound is developed (Figure 8). This central mound is underlain by a zone of chaotic and upturned stratal reflections extending downwards from ~2.4–2.7 s TWT, before transitioning into a wide (from ~1 to ~2 km) acoustically transparent zone >2.7 s TWT (Figure 8). A ~0.1 s TWT deep depression is located above the mound at the Marshall Paraconformity surface (Figure 8).

4.2.2 Interpretation

Based on the following lines of evidence we interpret that the mound-shaped features are buried volcanoes: i) the mound-shaped geometry of the structures atop a conformable base, and the likely conical morphology of the structures in plan-view, resembles volcano geometries observed in seismic reflection data elsewhere (e.g., Jackson, 2012; Magee et al., 2013; Reynolds et al., 2018; Morley, 2018) (Figure 2b; 8); ii) the positive amplitude seismic character of the mounds is consistent with a positive impedance contrast between igneous volcanic rocks and overlying sedimentary material (e.g., Magee et al., 2015); iii) where internal structures are resolved within the mounds, the reflections parallel the top surface, consistent with volcano construction via the proportional addition of material to their summit and flanks (e.g., Magee et al., 2013); and iv) onlapping of younger strata onto the mound-shaped feature flanks, which indicates the mounds were expressed at the surface and progressively buried, thereby discounting an origin as intrusions (e.g. laccoliths) emplaced in the subsurface. The anticlines observed above some volcanoes, which are not onlapped by overlying strata (i.e. they had no surface expression) but display amplitudes that progressively decay upwards

(e.g., Figure 6), likely represent later differential compaction folds (e.g., Holford et al., 2017; Sun et al., 2020). Differential compaction folds may form above volcanoes because volcanic rocks (e.g., crystalline lavas, volcanoclastics) cumulatively typically have a lower porosity than encasing and overlying, initially unconsolidated sedimentary material (e.g. Chopra and Marfurt, 2012). Upon burial, volcanoes therefore commonly compact less than the surrounding strata, promoting a differential compaction that results in the formation of anticlinal folds and associated outer-arc extension crestal faults above the volcano (e.g. Sun et al., 2020; Zhao et al., 2014), similar to those we describe here (Figure 6a, c, d).

The occurrence of flat tops on some volcanoes may be indicative of later erosion as they emerge at the paleo-seasurface (e.g., Bischoff et al., 2019; Bischoff et al., 2017), or may simply be a product of the volcano being intersected along its flank (not across its centre) by the 2D seismic lines. Sub-horizontal reflections within volcanoes may also correspond to the cut-effect of the seismic line sampling the flank of the structure. Although we are unable to determine the eruptive history of individual volcanoes, the distribution of multiple, relatively small volcanoes within a relatively localised area (typically 20-30 km from the centre of the Central edifice), suggests that they may represent a monogenetic volcanic field (Németh, 2010; Németh and White, 2003). Geometrically, the distribution of volcanoes bears similarities to that of the monogenetic Auckland Volcanic Field in the North Island (Cassidy and Locke, 2010; Le Corvec et al., 2013; Rout et al., 1993; Spörli and Eastwood, 1997), as well as monogenetic volcanic fields identified in seismic reflection data elsewhere (Bischoff et al., 2020; Bischoff et al., 2019; McLean et al., 2017).

Due to their clustering within and surrounding the Central edifice, we suggest that, at least for the upper parts of the domal edifice, the volcanoes may have been responsible for the eruption of the stacked lava packages, with the majority of activity occurring in the Paleocene. The volcanoes are located at different stratigraphic levels within the reflection package, with buried cones likely responsible for the eruption of older lavas (Figure 3, 6a). Additional volcanoes, and potential fissure vents, may be present at greater depths beneath the edifice although we are unable to resolve these structures due to a lack of imaging beneath the thick lava sequence (Quirie et al., 2019) (Figure 3).

To the south of the Central edifice, we interpret the small mound as a small, Early Eocene-aged volcano, with the adjacent high amplitude reflections interpreted as associated lava flows (Figure 8). This interpretation is corroborated by zone of chaotic and washed out reflectivity beneath the structure and the immediately adjacent upturned strata (Figure 8). The upturned strata are interpreted as a velocity pull-up, a seismic artefact generated due to relatively high velocities beneath the structure, suggestive of igneous material. The sub-vertical chaotic reflectivity beneath the volcano may correspond to igneous dykes or pipes, forming a vertical plumbing system to individual volcanoes (Figure 6f, 8) (Wall et al., 2010). The apparent small size of this cone may be a result of the seismic section only intersecting the margin of the structure, rather than passing through its centre (Figure 8). The volcano is associated with a series of Early Eocene high-amplitude reflections, which we interpret as erupted lava flows (Figure 8). The brightening of the lava flows away from the volcanic cone likely represents a decrease in thickness, and an associated increase in seismic tuning, towards their termination (Kallweit and Wood, 1982; Smallwood and Maresh, 2002; Widess, 1973) (Figure 8). The truncation of underlying strata by the lava flows may correspond to the formation of lava channels and the associated bulldozing and erosion of the underlying stratigraphy (Sun et al., 2019a). The onlapping of Early Eocene strata onto the lava flow may relate to the dominantly contouritic nature of the stratigraphy in this interval (Figure 1b). The depression on the Marshall Paraconformity surface co-located above the Early Eocene volcano cone appears to have formed due to fluid expulsion following burial of the volcano, which focussed migrating, non-volcanic-related fluids (Figure 8) (Holford et al., 2017; Sun et al., 2020). Buried volcanoes elsewhere have been shown to act as conduits for later fluid flow in the subsurface (Holford et al., 2017; Sun et al., 2020). We also interpret the sub-horizontal, high-amplitude reflection within the overlying differential compaction fold of one volcano as a ‘flat-spot’, likely corresponding to a trapped gas pocket (Figure 6e).

4.3 High-amplitude transgressive reflections

4.3.1 Observations

Aside from the high-amplitude, sub-horizontal reflection packages interpreted as lava flows, we identify 92 high-amplitude, positive polarity reflections that are laterally discontinuous and commonly display transgressive, saucer-shaped or inclined morphologies (Figure 9). These features typically have lengths ranging from 1-3 km, individually span depth ranges up to ~0.2 s TWT, and are observed at different stratigraphic levels between the pre-Coniacian and the Paleocene (Figure 7b, 9). Many of these transgressive high-amplitude reflections are located beneath interpreted volcanoes, although some appear independent of extrusive features and occur up to 30-40 km from the Central edifice (Figure 7b). The majority of these high-amplitude transgressive reflections are associated with clear anticlinal folds in the overlying strata, the outer inflection points of which directly overlie the lateral terminations of the high-amplitude reflection (Figure 9). These folds can be identified throughout Late Cretaceous-to-Early Eocene strata, with strata onlapping onto their margins (Figure 9).

4.3.2 Interpretation

We interpret these high-amplitude, transgressive reflections as igneous sills because: i) the high amplitude and positive reflection that defines their upper surface is consistent with an acoustically hard lithology, such as igneous material (Hansen et al., 2008); ii) they transgress and cross-cut background reflections, distinguishing these feature from the aforementioned lava flows, but do not offset strata and thus are not faults; and iii) their typical saucer-shaped geometry is similar to sheet intrusions identified onshore (Galerie et al., 2011; Ledevin et al., 2012; Polteau et al., 2008) and igneous sills resolved in seismic data, some of which have been drilled, from the Rockall Basin (Morewood et al., 2004; Thomson and Hutton, 2004), Faroe-Shetland Basin (McLean et al., 2017; Smallwood and Maresh, 2002), offshore Australia (Jackson, 2012; Magee et al., 2017; Magee et al., 2016), and in the Canterbury Basin offshore New Zealand (Bischoff et al., 2017; Reeves et al., 2018). We are able to relate the 92 high-amplitude features identified here as corresponding to ~79 individual sills, with some sills resolved across multiple seismic sections. Additional sills may be present beneath the main central dome, but they are not resolved in our data (Figure 3, 4, 7b). Overall, we classify the mapped intrusions as a sill-complex (Magee et al. 2016).

We interpret the folds overlying some of the sills as intrusion-induced forced folds that formed via overburden uplift to accommodate shallow-level magma emplacement (Hansen and Cartwright, 2006; Magee et al., 2013a; Reeves et al., 2018; Trude et al., 2003). Recognition of overlying strata onlapping onto these folds indicates the top fold surface corresponded to the syn-emplacement palaeosurface (Figure 9), and can be used to date intrusion (e.g. Trude et al., 2003). For those sills not overlain by forced folds we use the age of the encasing strata as a maximum estimate for emplacement timing; i.e. whilst ascending magma may arrest to form sills at any stratigraphic or structural level, in response to a range of different mechanisms (e.g., Kavanagh et al., 2006; Magee et al., 2016; Menand, 2011), its emplacement has to be younger than the host material age. We acknowledge that simply using host rock age to establish relative emplacement timings is not ideal because the mapped sills could be significantly younger than the rocks they intruded. Regardless, based on our defined maximum ages for sill emplacement and the seismic-stratigraphic onlap relationships, which allow to us accurately constrain emplacement age (e.g., Trude et al., 2003), we estimate sills ages within the Tuatara Volcanic Field range from the pre-Santonian (Top Teratan - >86.3 Ma) to Early Eocene (Top Heretaungan – 45.7 Ma), representing over 40 Myr of magmatic activity.

5 Distribution and age of volcano-magmatic structures in the Tuatara Volcanic Field

The Central edifice of the Tuatara Volcanic Field, which comprises stacked lava sequences, hyaloclastites, and volcanoes covers a ~270 km² elliptical area that is elongated in a NW-SE orientation (Figure 2); this part of the Tuatara Volcanic Field has been referred to as the Tapuku East volcanics (Bischoff et al., preprint). Igneous sills are much more widely distributed around the Central edifice than the volcanoes (Figure 7b). A subtle WNW-ESE trend is present in the spatial distribution of volcanoes and sills; this is more pronounced with the volcanoes (Figure 7). By determining the age of emplacement for the sills and volcanic cones, we assign these structures to stratigraphic intervals and examine how their distribution evolved temporally. Those volcanoes and sills emplaced prior to

the Santonian (>86.3 Ma) are typically located ~30 km to the southeast of the Central edifice, with some pre-Santonian aged sills also present northeast of the Central edifice (Figure 7). Late Cretaceous sills (from 86.3-66 Ma) are located closer to the Central edifice (~20 km) but distributed around its SW, SE, and NE sides (Figure 7b). No Late Cretaceous volcanoes were identified. Paleocene-aged structures are the most abundant across the area. Paleocene-aged volcanoes are relatively tightly clustered around the central dome compared to older volcanoes (~10 km) (Figure 7a). Paleocene sills are more proximal to the Central edifice relative to older sills, although they are still relatively distributed compared to volcanoes of the same age (Figure 7b). A cluster of Paleocene sills occur immediately west-northwest of the central dome. Early Eocene and younger sills and volcanoes occur to the northwest of the main edifice, with the exception of one sill straddling the Paleocene-Eocene boundary (Figure 9d), suggesting a broad north-westward migration of igneous activity from the pre-Santonian to the Early Eocene (Figure 7). The youngest structures, an Early Eocene sill (56-45.7 Ma) and a volcanoes younger than the Early Eocene (<45.7 Ma) (Figure 6b), are both located ~25-30 km to the northwest of the Central edifice, whereas the oldest interpreted structures are located approximately ~35 km to the southeast (Figure 7). Based on their overall clustering and age progression centred on the Central edifice we interpret the younger intrusions form part of the same volcanic system, focussed by the same mechanism as the older structures, as opposed to being part of an unrelated, later magmatic event (Bischoff et al., preprint).

The size, connectivity, and cumulative volume of the resolved sill-complex we map does not take into account the likely presence of thin sills, with thicknesses below the limits of visibility of the data (i.e. ≤ 7 m), which are difficult to identify in seismic reflection data (e.g., Eide et al., 2018; Schofield et al., 2017). Given that there are likely more sills present in the area than are resolved and that the mapped volcanoes and sills display a similar spatial and temporal distribution (Figure 7), with some intrusions seemingly extending up to the base of some volcanic edifices (e.g., Figure 6c), we suggest the sill-complex likely played a role in delivering magma to the surface. Inferring that the mapped sill-complex likely fed parts the Tuatara Volcanic Field implies some individual volcanoes may have been connected; i.e. activity at one volcano could have been linked to eruption at another as they

probably shared a plumbing system (Magee et al., 2016). We acknowledge that dykes or magma conduits that have since closed may be or have been present across the study area respectively, and probably contributed to the magma plumbing system. However, the expected sub-vertical geometry and thin nature of dykes, as well as that of closed conduits and associated remnant host rock changes (e.g. thermal aureoles), means that these structures are difficult to resolve on seismic reflection data (see Magee and Jackson, 2020 and references therein). Some volcanoes within the Tuatara Volcanic Field do appear to be underlain by pronounced vertical seismic disturbances, which we tentatively interpret as corresponding to dykes (Figure 6f, 7) (e.g., Magee and Jackson, 2020; Wall et al., 2010). In particular, these inferred dykes are largely resolved beneath, and appear to feed, isolated volcanic cones away from the central edifice (Figure 7a).

6 Discussion

The Tuatara Volcanic Field occupies a relatively localised ($\sim 270 \text{ km}^2$) setting above the Livingstone Fault, which marks the boundary between the Dun Mountain-Maitai Terrane to the south, and the Caples Terrane in the north (Figure 10) (Mortimer et al., 2002; Tarling et al., 2019). Here, we examine the controls on the localisation, geometry, and longevity of intraplate volcanic activity at the Tuatara Volcanic Field. We also discuss how our observations of the internal structure and plumbing system of the Tuatara Volcanic Field may relate to the Auckland Volcanic Field and enhance our understanding of intraplate volcanic systems generally.

6.1 Controls on the location of the Tuatara Volcanic Field

Intraplate volcanism appears to display a relatively random distribution across Zealandia (Bischoff et al., preprint; Hoernle et al., 2006; Timm et al., 2010); similar areas of diffuse intraplate volcanism have been identified across the Turkish-Iranian Plateau (Kaislaniemi et al., 2014). Such diffuse regions of intraplate volcanism have been related to decompression melting of upwelling asthenosphere into areas where Rayleigh-Taylor instabilities and/or small-scale mantle convection, which occur due to density contrasts at the lithosphere-asthenosphere boundary and/or hydrated

mantle following protracted subduction, has detached lithospheric material (Elkins-Tanton, 2005; Hoernle et al., 2006; Kaislaniemi et al., 2014). According to these models, intraplate volcanic systems are located directly above the seemingly randomly distributed areas of detaching lithosphere and associated decompression melting (Elkins-Tanton, 2005; Hoernle et al., 2006; Kaislaniemi et al., 2014). However, because some volcanic systems, such as those on the Chatham Islands and Banks Peninsula, display repeated phases of activity with long intervening periods (Figure 1) (Hoernle et al., 2006; Timm et al., 2009), it is necessary to consider how localised areas of lithospheric detachment and volcanic activity could be rejuvenated.

We consider lithospheric detachment as the likely mechanism for activity at the Tuatara Volcanic Field, which we suggest is reflected in its elliptical geometry, similar to that of the Auckland Volcanic Field; i.e. the areal extent of the Tuatara Volcanic Field likely marks the limits of an underlying zone of melt where the lithosphere detached (Le Corvec et al., 2013; Spörli and Eastwood, 1997).

However, we also note that the Tuatara Volcanic Field overlies the Livingstone Fault, which marks the boundary between the Caples and Dun Matai terranes. The Auckland Volcanic Field and volcanoes on the Banks Peninsula are also co-located along prominent basement terrane boundaries, namely the same boundary as the Tuatara Volcanic Field, between the Dun Mountain-Maitai and Caples terranes, and the Rakaia and Pahau terranes respectively (Figure 1a) (Eccles et al., 2005; Mortimer et al., 2002; Tarling et al., 2019). This co-location of volcanic fields with major basement terrane boundaries questions whether the localisation of intraplate volcanic systems may, at least partially, be controlled by pre-existing structures. For example, faults have been shown to act as conduits for magma and may thus spatially correlate with the plumbing systems of volcanoes (e.g. Mazzarini, 2007). Based on the overall location of the Tuatara Volcanic Field and the approximate NW-alignment of constituent volcanoes and sills, parallel to the underlying basement terranes and Livingstone Fault (Figure 2b), we suggest that the location of the Tuatara Volcanic Field was primarily controlled by underlying pre-existing structures. In particular, we envisage that the Livingstone Fault, and perhaps sub-vertical foliations within the Dun Mountain-Matai terrane,

provided viable pathways for magma ascending through the crust (Eccles et al., 2005; Hopkins et al., 2020).

Considering the location of the Tuatara Volcanic Field is linked to that of the Livingstone Fault at upper crustal depths, we in turn question whether the site of lithosphere detachment could have been influenced by pre-existing structures. Regional seismic reflection data located offshore of the South Island indicate that the Livingstone Fault extends down to at least the Moho (Figure 1, 10c) (Mortimer et al., 2002). If the Dun Mountain-Matai and Caples terranes, which accreted to the southern margin of Gondwana, are characterised by different lithospheric thicknesses and properties, we suggest that the Livingstone Fault could extend deeper and have some expression at the base of the lithosphere (i.e. a change in lithospheric thickness or narrow keel; Figure 10c) (Eccles et al., 2005; Tarling et al., 2019). Such promontories at the base of the lithosphere may provide a first-order control on the development of small-scale mantle convection cells and Rayleigh-Taylor instabilities, focussing the detachment of lithospheric material (Figure 10c). Elsewhere, small-scale convection cells will be controlled by the spacing between adjacent cells, causing lithosphere detachment and the associated intraplate volcanic systems to not be ‘directly’ related to a pre-existing structure and appear randomly distributed (Kaislaniemi et al., 2014). Therefore, whilst pre-existing structures appear to control, or at least influence, the location of some individual intraplate volcanic systems (e.g., the Tuatara Volcanic Field), it also allows for a random background distribution of intraplate volcanic systems that bear no apparent relation to pre-existing structure.

Although spatial correlation suggests the location of the Tuatara Volcanic Field as a whole was influenced by pre-existing structures, it is difficult to ascertain whether its individual intrusive or extrusive components were similarly structurally controlled. For example, at shallow depths within the Tuatara Volcanic Field, we are unable to fully constrain the geometry of rift-related faults beneath the Central edifice, although faults typically strike NE-SW across the Great South and Canterbury Basins (Phillips and McCaffrey, 2019; Uruski et al., 2007; Uruski, 2010). Overall, we suggest the transition from vertical magma ascent from the base of the lithosphere, likely via dykes, to apparently favour the formation of a sill-complex within the Great South Basin may have been related to a local

change in the differential stress field at shallower depths (Stephens et al., 2017), and/or deflection of magma pathways along sub-horizontal boundaries (Kavanagh et al., 2006; Kenny et al., 2012).

6.2 Controls on the longevity of the Tuatara Volcanic Field

The longevity of intraplate volcanic systems across Zealandia (i.e. those not related to rift activity) is proposed to be determined by the time taken for the area of material detached from the base of the lithosphere to anneal, thereby stopping any decompression melting of upwelling asthenosphere (Timm et al., 2009). Accordingly, the larger the diameter and depth of the volume of detached lithosphere, the greater the expected magmatism, either in magnitude or longevity. The magnitude of melting in turn influences the resultant style of volcanism; low-Si monogenetic volcanic fields are thought to relate to small areas of detaching lithosphere producing small-degree melts with larger shield volcanoes (i.e. those at Banks Peninsula) associated with larger and deeper areas of detaching lithosphere producing larger-degrees of melting (Hoernle et al., 2006).

We document a ~40 Myr record of magmatic and volcanic activity across the Tuatara Volcanic Field lasting from ~85–45 Ma. Earlier volcano-magmatic features may be present at deeper levels, although we are unable to resolve structures at these depths (Figure 3, 4). The earliest phases of activity in the Tuatara Volcanic Field appear to post-date the cessation of subduction along the southern margin of Gondwana caused by impingement of the Hikurangi Plateau (Davy et al., 2008), and overlap with rifting associated with Gondwana breakup, which lasted until ~80 Ma (Kula et al., 2007; Tulloch et al., 2019). The vast majority of volcano-magmatic activity in the Tuatara Volcanic Field and across Zealandia occurred in an intraplate setting, with the main period of activity during the Paleocene (Figure 10a).

The ages of sills and volcanoes identified within the Tuatara Volcanic Field migrates towards the northwest through time, following the orientation of the underlying basement terranes (Figure 7). Similarly, at the Banks Peninsula on the South Island, volcanic activity migrates along the NW-trending boundary between the Pahau and Rakaia terranes, albeit migrating in the opposite direction to that observed at the Tuatara Volcanic Field. Volcanic activity initially occurs at the Lyttelton

Volcano in the northwest (12.3-10.4 Ma), before migrating to the Akaroa Volcano ~25 km southeast (9.4-6.8 Ma), correlating to the NW-trending terrane boundary between the Pahau and Rakaia terranes, (Timm et al., 2009). In the case of Banks Peninsula, this may reflect progressive lithosphere detachment towards the southeast along the terrane boundary; as the lithosphere begins to anneal beneath the Lyttelton Volcano, further detachment occurs to the southeast leading to activity at the Akaroa Volcano (Timm et al., 2009). We propose a similar mechanism of along-strike progressive lithospheric detachment focused along the expression of the Livingstone Fault at the lithosphere-asthenosphere boundary to explain the longevity and age progression within the Tuatara Volcanic Field (Figure 11) (Mortimer, 2004). In particular, we suggest such localisation by pre-existing structures may result in a quasi-periodic ‘dripping’ of material from the base of the lithosphere, focussing magmatic upwelling and inhibiting the complete annealing of the lithosphere over prolonged (>10 Myr) periods. That monogenetic volcanic fields are typically characterised by small-degree melts (Hoernle et al., 2006; Timm et al., 2009) suggests this quasi-periodic dripping is involves relatively small, but relatively frequent detaching of lithospheric material.

6.3 Implications for intraplate volcanism

We document the 3D geometry and longevity of an intraplate volcanic system, highlighting that seismic reflection data can potentially provide important insights into the processes driving intraplate volcanism. To explore the applicability of our findings to other examples of intraplate volcanism across New Zealand, we here compare to similar volcanic fields occur in the same structural setting on the North Island, where basement terranes are offset along the Alpine Fault (Figure 1a). There is a northwards younging of volcanic fields along the Dun Mountain ophiolite belt in the North Island; from the Okete volcanic field in the south (2.69–1.8Ma), northwards to the Ngatutura (1.83–1.54Ma), South Auckland (1.59–0.51Ma), and the recently active Auckland Volcanic Field (193 Ka–500 yr BP) (Hopkins et al., 2020). In particular, we find that, the recently active (last eruption 500 yr before present) Auckland Volcanic Field on the North Island is situated in the same structural setting, i.e. above the terrane boundary between the Dun-Mountain-Maitai and Caples terranes represented by the Livingstone Fault, as the Tuatara Volcanic Field on the opposite side of the Alpine Fault on the South

Island (Figure 1a, 10b) (e.g. Cassidy and Locke, 2010; Lindsay et al., 2011; McGee et al., 2013; Rout et al., 1993; Spörli et al., 2015; Tarling et al., 2019). Both volcanic fields display similar geometric characteristics at the surface: the Auckland Volcanic Field is characterised by ~50 individual volcanic centres (each typically ~1–2 km in diameter) distributed across a roughly elliptical area with a ~29 km long axis and a short axis of ~16 km (~375 km²) (Hopkins et al., 2020; Le Corvec et al., 2013; Lindsay et al., 2011; Spörli and Eastwood, 1997); this is compared to 69 volcanoes (typically 1–2 km in diameter) identified within the 23 km x 15 km (~270 km²) Tuatara Volcanic Field. The Tuatara Volcanic Field may thus represent a crucial ancient analogue to the Auckland Volcanic Field, potentially helping to constrain our understanding of the currently uncertain magma plumbing system and subsurface geology of the latter. In particular, the shallow-level plumbing system of the Tuatara Volcanic Field involves interconnected sills (Figure 6f). If the Auckland Volcanic Field also comprises a shallow-level, sill-complex, in addition to dykes, it is plausible that individual volcanoes could be linked such that (Magee et al., 2016): (i) activity at one could instigate activity at another; and/or (ii) pre-eruption warning signals (e.g., ground deformation and seismicity) may be laterally offset from the subsequent eruption site. Our work also implies that extinct volcanoes may be buried beneath the current exposure of the Auckland Volcanic Field; these buried volcanoes could provide pathways for fluid/gas escape (e.g., Figure 6b) (e.g., Holford et al., 2017; Sun et al., 2020). Finally, whilst we are unable to directly comment on the likely longevity of volcanic activity in the Auckland Volcanic Field, observations from the Tuatara Field described here suggest that volcanic fields partly controlled by pre-existing structures could periodically be rejuvenated. Overall, hazard assessment of the Auckland Volcanic Field should take into account potential constraints on the location, geometry, and longevity of the system afforded by our study of the analogue Tuatara Volcanic Field.

7 Conclusions

We use seismic reflection data to image and document a newly discovered volcanic field, which we name the Tuatara Volcanic Field, located in the Great South Basin, offshore of the South Island of

New Zealand. The ~270 km² Tuatara Volcanic Field is characterised by a central edifice comprising stacked lava and hyaloclastite sequences surrounded by 69 volcanoes connected by a sill-complex; we consider dykes also play an important role in the plumbing system but these are not imaged in our data. Igneous activity occurred periodically over 40 Myr, beginning after rifting in the Late Cretaceous (~85 Ma) and continuing until the Early-to-Mid Eocene (~45 Ma). The Tuatara Volcanic Field thus represents one of the longest-lived volcanic systems in Zealandia and potentially elsewhere. The location of the Tuatara Volcanic Field coincides with the Livingstone Fault, a crustal-to-lithosphere scale boundary between the Dun Mountain-Maitai and Caples terranes, which we suggest facilitated magma ascent. Activity within the field migrates towards the northwest and to higher stratigraphic levels through time, following the orientation of the underlying basement structure. We suggest that the Livingstone Fault had some expression at the base of the lithosphere, which periodically promoted detachment of material from the lithosphere by Rayleigh-Taylor instabilities and/or small-scale mantle convection. Decompression melting of upwelling asthenosphere into this area of detached lithosphere likely controlled the site of the Tuatara Volcanic Field. Where such pre-existing structures are absent, lithosphere detachment and intraplate volcanism may occur randomly and display shorter periods of activity.

The geometry and structural setting of the Tuatara Volcanic Field resembles the Auckland Volcanic Field; the locations of both volcanic fields appear to be controlled by the pre-existing Livingstone Fault and terrane boundary. We suggest that the Tuatara Volcanic Field represents an ancient analogue to the Auckland Volcanic Field. Our observations of the internal structure and longevity of the Tuatara Volcanic Field may thus provide important insight into potential future activity at the Auckland Volcanic Field. In particular, whilst magma transport is dominantly vertical throughout the lithosphere, the plumbing system of the Auckland Volcanic Field may include a sill-complex that could connect and control the distribution of volcanoes within the field. Furthermore, we postulate that the longevity and progression of activity at the Tuatara Volcanic Field could imply that the Auckland Volcanic Field is perhaps relatively early in its evolution and that activity may migrate along the pre-existing structure across geological time. In this study, we have characterised the

internal plumbing system of a volcanic system offshore New Zealand. We highlight how pre-existing crustal and lithospheric structure exert an important influence over the location and longevity of individual intraplate volcanic systems. We offer insights into the internal structure and plumbing system of these volcanic fields that may be applicable to other ancient and active intraplate systems.

Acknowledgements

The authors would like to thank the Leverhulme Trust for funding an Early Career Fellowship for Phillips. Magee is funded by a NERC independent research fellowship. The authors would also like to thank New Zealand Petroleum and Minerals for making the seismic reflection data used in this study publically available, and Schlumberger for providing access to academic licences for Petrel software. We also thank Francesco Mazzarini and an anonymous reviewer for reviewing the manuscript, and Tyrone Rooney for editorial handling.

Funding

This project is funded by a Leverhulme Early Career Fellowship provided to Phillips at the University of Durham.

References

- Acocella, V., Spinks, K., Cole, J., Nicol, A., 2003. Oblique back arc rifting of Taupo Volcanic Zone, New Zealand. *Tectonics* 22.
- Adams, C.J., 1983. Age of the volcanoes and granite basement of the Auckland Islands, Southwest Pacific. *New Zealand Journal of Geology and Geophysics* 26, 227-237.
- Adams, R.D., 1962. Thickness of the earth's crust beneath the Campbell Plateau. *New Zealand Journal of Geology and Geophysics* 5, 74-85.
- Beggs, J., 1993. Depositional and tectonic history of the Great South Basin. *South Pacific sedimentary basins. Sedimentary basins of the World* 2, 365-373.

765 Bertoni, C., Gan, Y., Paganoni, M., Mayer, J., Cartwright, J., Martin, J., Van Rensbergen, P.,
766 Wunderlich, A., Clare, A., 2019. Late Paleocene pipe swarm in the Great South – Canterbury
767 Basin (New Zealand). *Marine and Petroleum Geology* 107, 451-466.

768 Bischoff, A., Barrier, A., Beggs, M., Nicol, A., Cole, J., Sahoo, T., Preprint. Magmatic and
769 Tectonic Interactions in Te Riu-a-Māui/Zealandia Sedimentary Basins.
770 10.13140/RG.2.2.33641.24166

771 Bischoff, A., Nicol, A., Barrier, A., Wang, H., 2020. Characterization of a Middle Miocene
772 Monogenetic Volcanic Field Buried in the Canterbury Basin, New Zealand – Part II.

773 Bischoff, A., Nicol, A., Rossetti, M., Kennedy, B., 2019. Characterization of a Middle
774 Miocene Monogenetic Volcanic Field Buried in the Canterbury Basin, New Zealand – Part I.
775 EarthArXiv.

776 Bischoff, A.P., Nicol, A., Beggs, M., 2017. Stratigraphy of architectural elements in a buried
777 volcanic system and implications for hydrocarbon exploration. *Interpretation* 5, SK141-
778 SK159.

779 Bishop, D., Bradshaw, J., Landis, C., 1985. Provisional terrane map of South Island, New
780 Zealand.

781 Brown, A.R., 2011. Interpretation of three-dimensional seismic data. *Society of Exploration*
782 *Geophysicists and American Association of Petroleum*

783 Buntin, S., Malehmir, A., Koyi, H., Högdahl, K., Malinowski, M., Larsson, S.Å., Thybo, H.,
784 Juhlin, C., Korja, A., Górszczyk, A., 2019. Emplacement and 3D geometry of crustal-scale
785 saucer-shaped intrusions in the Fennoscandian Shield. *Scientific Reports* 9, 10498.

786 Calvès, G., Schwab, A.M., Huuse, M., Clift, P.D., Gaina, C., Jolley, D., Tabrez, A.R., Inam,
787 A., 2011. Seismic volcanostratigraphy of the western Indian rifted margin: The pre-Deccan
788 igneous province. *Journal of Geophysical Research: Solid Earth* 116.

789 Cassidy, J., Locke, C.A., 2010. The Auckland volcanic field, New Zealand: Geophysical
790 evidence for structural and spatio-temporal relationships. *Journal of Volcanology and*
791 *Geothermal Research* 195, 127-137.

792 Chenrai, P., Huuse, M., 2020. Sand injection and polygonal faulting in the Great South Basin,
793 New Zealand. *Geological Society, London, Special Publications* 493, SP493-2018-2107.

794 Chopra, S., Marfurt, K.J., 2012. Seismic attribute expression of differential compaction. *The*
795 *Leading Edge* 31, 1418-1422.

796 Clague, D.A., Jarrard, R.D., 1973. Tertiary Pacific Plate Motion Deduced from the Hawaiian-
797 Emperor Chain. *GSA Bulletin* 84, 1135-1154.

798 Clouard, V., Bonneville, A., 2005. Ages of seamounts, islands, and plateaus on the Pacific
799 plate. *Special Papers-Geological Society of America* 388, 71.

800 Collanega, L., Jackson, C.A.L., Bell, R.E., Coleman, A.J., Lenhart, A., Breda, A., 2018.
801 Normal fault growth influenced by basement fabrics: the importance of preferential
802 nucleation from pre-existing structures. *Basin Res* 0.

803 Cooper, A.F., Barreiro, B.A., Kimbrough, D.L., Mattinson, J.M., 1987. Lamprophyre dike
804 intrusion and the age of the Alpine fault, New Zealand. *Geology* 15, 941-944.

805 Cooper, A.F., Norris, R.J., 1994. Anatomy, structural evolution, and slip rate of a plate-
806 boundary thrust: The Alpine fault at Gaunt Creek, Westland, New Zealand. *GSA Bulletin*
807 106, 627-633.

808 Davey, F.J., Christoffel, D.A., 1978. Magnetic anomalies across Campbell Plateau, New
809 Zealand. *Earth and Planetary Science Letters* 41, 14-20.

810 Davies, D.R., Rawlinson, N., Iaffaldano, G., Campbell, I.H., 2015. Lithospheric controls on
811 magma composition along Earth's longest continental hotspot track. *Nature* 525, 511.

812 Davy, B., Hoernle, K., Werner, R., 2008. Hikurangi Plateau: Crustal structure, rifted
813 formation, and Gondwana subduction history. *Geochemistry, Geophysics, Geosystems* 9.

814 Eccles, J.D., Cassidy, J., Locke, C.A., Spörli, K.B., 2005. Aeromagnetic imaging of the Dun
815 Mountain Ophiolite Belt in northern New Zealand: insight into the fine structure of a major
816 SW Pacific terrane suture. *Journal of the Geological Society* 162, 723.

817 Eide, C.H., Schofield, N., Lecomte, I., Buckley, S.J., Howell, J.A., 2018. Seismic
818 interpretation of sill complexes in sedimentary basins: implications for the sub-sill imaging
819 problem. *Journal of the Geological Society* 175, 193-209.

820 Elkins-Tanton, L.T., 2005. Continental magmatism caused by lithospheric delamination, in:
821 Foulger, G.R., Natland, J.H., Presnall, D.C., Anderson, D.L. (Eds.), *Plates, plumes and*
822 *paradigms*. Geological Society of America, p. 0.

823 Finn, C.A., Müller, R.D., Panter, K.S., 2005. A Cenozoic diffuse alkaline magmatic province
824 (DAMP) in the southwest Pacific without rift or plume origin. *Geochemistry, Geophysics,*
825 *Geosystems* 6.

826 Fulthorpe, C.S., Carter, R.M., Miller, K.G., Wilson, J., 1996. Marshall Paraconformity: a
827 mid-Oligocene record of inception of the Antarctic circumpolar current and coeval glacio-
828 eustatic lowstand? *Marine and Petroleum Geology* 13, 61-77.

829 Galerne, C.Y., Galland, O., Neumann, E.-R., Planke, S., 2011. 3D relationships between sills
830 and their feeders: evidence from the Golden Valley Sill Complex (Karoo Basin) and
831 experimental modelling. *Journal of Volcanology and Geothermal Research* 202, 189-199.

832 Gallagher, J.W., Dromgoole, P.W., 2007. Exploring below the basalt, offshore Faroes: a case
833 history of sub-basalt imaging. *Petroleum Geoscience* 13, 213.

834 Grindley, G.W., Adams, C.J.D., Lumb, J.T., Watters, W.A., 1977. Paleomagnetism, K-Ar
835 dating and tectonic interpretation of Upper Cretaceous and Cenozoic volcanic rocks of the
836 Chatham Islands, New Zealand. *New Zealand Journal of Geology and Geophysics* 20, 425-
837 467.

838 Grobys, J.W.G., Gohl, K., Uenzelmann-Neben, G., Davy, B., Barker, D., 2009. Extensional
839 and magmatic nature of the Campbell Plateau and Great South Basin from deep crustal
840 studies. *Tectonophysics* 472, 213-225.

841 Hansen, D.M., Cartwright, J., 2006. The three-dimensional geometry and growth of forced
842 folds above saucer-shaped igneous sills. *Journal of Structural Geology* 28, 1520-1535.

843 Hansen, D.M., Redfern, J., Federici, F., di Biase, D., Bertozzi, G., 2008. Miocene igneous
844 activity in the Northern Subbasin, offshore Senegal, NW Africa. *Marine and Petroleum*
845 *Geology* 25, 1-15.

846 Higgs, K.E., Browne, G.H., Sahoo, T.R., 2019. Reservoir characterisation of syn-rift and
847 post-rift sandstones in frontier basins: An example from the Cretaceous of Canterbury and
848 Great South basins, New Zealand. *Marine and Petroleum Geology* 101, 1-29.

849 Hoernle, K., White, J.D.L., van den Bogaard, P., Hauff, F., Coombs, D.S., Werner, R., Timm,
850 C., Garbe-Schönberg, D., Reay, A., Cooper, A.F., 2006. Cenozoic intraplate volcanism on
851 New Zealand: Upwelling induced by lithospheric removal. *Earth and Planetary Science*
852 *Letters* 248, 350-367.

853 Holford, S.P., Schofield, N., Reynolds, P., 2017. Subsurface fluid flow focused by buried
854 volcanoes in sedimentary basins: Evidence from 3D seismic data, Bass Basin, offshore
855 southeastern Australia. *Interpretation* 5, SK39-SK50.

856 Hopkins, J.L., Smid, E.R., Eccles, J.D., Hayes, J.L., Hayward, B.W., McGee, L.E. van Wijk,
857 K., Wilson, T.M., Cronin, S.J., Leonard, G.S., Lindsay, J.M., Németh, K., Smith, I.E.M.,
858 2020. Auckland Volcanic Field magmatism, volcanism, and hazard: a review, *New Zealand*
859 *Journal of Geology and Geophysics*, DOI: 10.1080/00288306.2020.1736102

860 Howell, D.G., 1980. Mesozoic accretion of exotic terranes along the New Zealand segment of
861 Gondwanaland. *Geology* 8, 487-491.

862 Hunt, T., 1978. Stokes magnetic anomaly system. *New Zealand journal of geology and*
863 *geophysics* 21, 595-606.

864 Jackson, C.A.L., 2012. Seismic reflection imaging and controls on the preservation of ancient
865 sill-fed magmatic vents. *Journal of the Geological Society* 169, 503.

866 Johnston, M.R., 2019. Chapter 2 The path to understanding the central terranes of
867 Zealandia. Geological Society, London, Memoirs 49, 15-30.

868 Kaislaniemi, L., van Hunen, J., Allen, M.B., Neill, I., 2014. Sublithospheric small-scale
869 convection—A mechanism for collision zone magmatism. *Geology* 42, 291-294.

870 Kallweit, R.S., Wood, L.C., 1982. The limits of resolution of zero-phase wavelets.
871 *Geophysics* 47, 1035-1046.

872 Kavanagh, J.L., Menand, T., Sparks, R.S.J., 2006. An experimental investigation of sill
873 formation and propagation in layered elastic media. *Earth and Planetary Science Letters* 245,
874 799-813.

875 Kenny, J.A., Lindsay, J.M., Howe, T.M., 2012. Post-Miocene faults in Auckland: insights
876 from borehole and topographic analysis. *New Zealand Journal of Geology and Geophysics*
877 55, 323-343.

878 Killops, S.D., Cook, R.A., Sykes, R., Boudou, J.P., 1997. Petroleum potential and oil-source
879 correlation in the Great South and Canterbury Basins. *New Zealand Journal of Geology and*
880 *Geophysics* 40, 405-423.

881 Kula, J., Tulloch, A., Spell, T.L., Wells, M.L., 2007. Two-stage rifting of Zealandia-
882 Australia-Antarctica: Evidence from $^{40}\text{Ar}/^{39}\text{Ar}$ thermochronometry of the Sisters shear
883 zone, Stewart Island, New Zealand. *Geology* 35, 411-414.

884 Laird, M.G., Bradshaw, J.D., 2004. The Break-up of a Long-term Relationship: the
885 Cretaceous Separation of New Zealand from Gondwana. *Gondwana Research* 7, 273-286.

886 Lamb, S., Mortimer, N., Smith, E., Turner, G., 2016. Focusing of relative plate motion at a
887 continental transform fault: Cenozoic dextral displacement >700 km on New Zealand's
888 Alpine Fault, reversing >225 km of Late Cretaceous sinistral motion. *Geochemistry,*
889 *Geophysics, Geosystems* 17, 1197-1213.

890 Le Corvec, N., Bebbington, M. S., Lindsay, J. M., and McGee, L. E. (2013), Age, distance,
891 and geochemical evolution within a monogenetic volcanic field: Analyzing patterns in the
892 Auckland Volcanic Field eruption sequence, *Geochem. Geophys. Geosyst.*, 14, 3648– 3665,
893 doi:10.1002/ggge.20223.

894 Ledevin, M., Arndt, N., Cooper, M.R., Earls, G., Lyle, P., Aubourg, C., Lewin, E., 2012.
895 Intrusion history of the Portrush Sill, County Antrim, Northern Ireland: evidence for rapid
896 emplacement and high-temperature contact metamorphism. *Geological Magazine* 149, 67-79.

897 Lindsay, J.M., Leonard, G.S., Smid, E.R., Hayward, B.W., 2011. Age of the Auckland
898 Volcanic Field: a review of existing data. *New Zealand Journal of Geology and Geophysics*
899 54, 379-401.

900 Lu, H., Fulthorpe, C.S., 2004. Controls on sequence stratigraphy of a middle Miocene–
901 Holocene, current-swept, passive margin: Offshore Canterbury Basin, New Zealand. *GSA*
902 *Bulletin* 116, 1345-1366.

903 Magee, C., Briggs, F., Jackson, C.A.L., 2013a. Lithological controls on igneous intrusion-
904 induced ground deformation. *Journal of the Geological Society* 170, 853.

905 Magee, C., Ernst, R.E., Muirhead, J., Phillips, T., Jackson, C.A.-L., 2019. Magma Transport
906 Pathways in Large Igneous Provinces: Lessons from Combining Field Observations and
907 Seismic Reflection Data, *Dyke Swarms of the World: A Modern Perspective*. Springer, pp.
908 45-85.

909 Magee, C., Hunt-Stewart, E., Jackson, C.A.L., 2013b. Volcano growth mechanisms and the
910 role of sub-volcanic intrusions: Insights from 2D seismic reflection data. *Earth and Planetary*
911 *Science Letters* 373, 41-53.

912 Magee, C., Jackson, C.A.-L., How do normal faults grow above dykes? *EarthArXiv*.

913 Magee, C., Jackson, C.A.L., 2020. Seismic reflection data reveal the 3D structure of the
914 newly discovered Exmouth Dyke Swarm, offshore NW Australia. *EarthArXiv*.

915 Magee, C., Jackson, C.A.L., Hardman, J.P., Reeve, M.T., 2017. Decoding sill emplacement
916 and forced fold growth in the Exmouth Sub-basin, offshore northwest Australia: Implications
917 for hydrocarbon exploration. *Interpretation* 5, SK11-SK22.

918 Magee, C., Maharaj, S.M., Wrona, T. and Jackson, C.A.L., 2015. Controls on the expression
919 of igneous intrusions in seismic reflection data. *Geosphere*, 11(4), pp.1024-1041.
920 doi:10.1130/GES01150.1

921 Magee, C., Muirhead, J.D., Karvelas, A., Holford, S.P., Jackson, C.A.L., Bastow, I.D.,
922 Schofield, N., Stevenson, C.T.E., McLean, C., McCarthy, W., Shtukert, O., 2016. Lateral
923 magma flow in mafic sill complexes. *Geosphere* 12, 809-841.

924 Magee, C., Stevenson, C.T.E., Ebmeier, S.K., Keir, D., Hammond, J.O.S., Gottsmann, J.H.,
925 Whaler, K.A., Schofield, N., Jackson, C.A.L., Petronis, M.S., O'Driscoll, B., Morgan, J.,
926 Cruden, A., Vollgger, S.A., Dering, G., Micklethwaite, S., Jackson, M.D., 2018. Magma
927 Plumbing Systems: A Geophysical Perspective. *Journal of Petrology* 59, 1217-1251.

928 Maresh, J., White, R.S., Hobbs, R.W., Smallwood, J.R., 2006. Seismic attenuation of Atlantic
929 margin basalts: Observations and modeling. *Geophysics* 71, B211-B221.

930 Mazzarini, F., 2007. Vent distribution and crustal thickness in stretched continental crust: The
931 case of the Afar Depression (Ethiopia). *Geosphere* 3, 152-162.

932 McGee, L.E., Smith, I.E.M., Millet, M.-A., Handley, H.K., Lindsay, J.M., 2013.
 933 Asthenospheric Control of Melting Processes in a Monogenetic Basaltic System: a Case
 934 Study of the Auckland Volcanic Field, New Zealand. *Journal of Petrology* 54, 2125-2153.

935 McLean, C.E., Schofield, N., Brown, D.J., Jolley, D.W., Reid, A., 2017. 3D seismic imaging
 936 of the shallow plumbing system beneath the Ben Nevis Monogenetic Volcanic Field: Faroe–
 937 Shetland Basin. *Journal of the Geological Society* 174, 468.

938 Menand, T., 2011. Physical controls and depth of emplacement of igneous bodies: A
 939 review. *Tectonophysics*, 500(1-4), pp.11-19.

940 Morewood, N.C., Shannon, P.M., Mackenzie, G.D., 2004. Seismic stratigraphy of the
 941 southern Rockall Basin: a comparison between wide-angle seismic and normal incidence
 942 reflection data. *Marine and Petroleum Geology* 21, 1149-1163.

943 Morgan, W.J., 1972. Deep mantle convection plumes and plate motions. *AAPG bulletin* 56,
 944 203-213.

945 Morley, C.K., 2018. 3-D seismic imaging of the plumbing system of the Kora Volcano,
 946 Taranaki Basin, New Zealand: The influence of syn-rift structure on shallow igneous
 947 intrusion architecture. *Geosphere* 14, 2533-2584.

948 Morley, C.K., Maczak, A., Rungprom, T., Ghosh, J., Cartwright, J.A., Bertoni, C.,
 949 Panpichityota, N., 2017. New style of honeycomb structures revealed on 3D seismic data
 950 indicate widespread diagenesis offshore Great South Basin, New Zealand. *Marine and*
 951 *Petroleum Geology* 86, 140-154.

952 Mortimer, N., 2004. New Zealand's Geological Foundations. *Gondwana Research* 7, 261-
 953 272.

954 Mortimer, N., Davey, F.J., Melhuish, A., Yu, J., Godfrey, N.J., 2002. Geological
 955 interpretation of a deep seismic reflection profile across the Eastern Province and Median
 956 Batholith, New Zealand: Crustal architecture of an extended Phanerozoic convergent orogen.
 957 *New Zealand Journal of Geology and Geophysics* 45, 349-363.

958 Mortimer, N., Rattenbury, M.S., King, P.R., Bland, K.J., Barrell, D.J.A., Bache, F., Begg,
 959 J.G., Campbell, H.J., Cox, S.C., Crampton, J.S., Edbrooke, S.W., Forsyth, P.J., Johnston,
 960 M.R., Jongens, R., Lee, J.M., Leonard, G.S., Raine, J.I., Skinner, D.N.B., Timm, C.,
 961 Townsend, D.B., Tulloch, A.J., Turnbull, I.M., Turnbull, R.E., 2014. High-level stratigraphic
 962 scheme for New Zealand rocks. *New Zealand Journal of Geology and Geophysics* 57, 402-
 963 419.

964 Mortimer, N., Tulloch, A.J., Spark, R.N., Walker, N.W., Ladley, E., Allibone, A.,
 965 Kimbrough, D.L., 1999. Overview of the Median Batholith, New Zealand: a new
 966 interpretation of the geology of the Median Tectonic Zone and adjacent rocks. *Journal of*
 967 *African Earth Sciences* 29, 257-268.

968 Mortimer, N., van den Bogaard, P., Hoernle, K., Timm, C., Gans, P.B., Werner, R., Riefstahl,
969 F., 2019. Late Cretaceous oceanic plate reorganization and the breakup of Zealandia and
970 Gondwana. *Gondwana Research* 65, 31-42.

971 Muir, R.J., Bradshaw, J.D., Weaver, S.D., Laird, M.G., 2000. The influence of basement
972 structure on the evolution of the Taranaki Basin, New Zealand. *Journal of the Geological*
973 *Society* 157, 1179.

974 Németh, K., 2010. Monogenetic volcanic fields: Origin, sedimentary record, and relationship
975 with polygenetic volcanism, in: Cañón-Tapia, E., Szakács, A. (Eds.), *What Is a Volcano?*
976 *Geological Society of America*, p. 0.

977 Németh, K., White, J.D.L., 2003. Reconstructing eruption processes of a Miocene
978 monogenetic volcanic field from vent remnants: Waipiata Volcanic Field, South Island, New
979 Zealand. *Journal of Volcanology and Geothermal Research* 124, 1-21.

980 Németh, K., White, J.D.L., Reay, A., Martin, U., 2003. Compositional variation during
981 monogenetic volcano growth and its implications for magma supply to continental volcanic
982 fields. *Journal of the Geological Society* 160, 523.

983 Patruno, S., Helland-Hansen, W., 2018. Clinoforms and clinoform systems: Review and
984 dynamic classification scheme for shorelines, subaqueous deltas, shelf edges and continental
985 margins. *Earth-Science Reviews* 185, 202-233.

986 Phillips, T.B., McCaffrey, K.J., 2019. Terrane boundary reactivation, barriers to lateral fault
987 propagation and reactivated fabrics - Rifting across the Median Batholith Zone, Great South
988 Basin, New Zealand. *Tectonics* 0.

989 Planke, S., Rasmussen, T., Rey, S.S., Myklebust, R., 2005. Seismic characteristics and
990 distribution of volcanic intrusions and hydrothermal vent complexes in the Vøring and Møre
991 basins. *Geological Society, London, Petroleum Geology Conference*
992 series 6, 833.

993 Planke, S., Symonds, P.A., Alvestad, E., Skogseid, J., 2000. Seismic volcanostratigraphy of
994 large-volume basaltic extrusive complexes on rifted margins. *Journal of Geophysical*
995 *Research: Solid Earth* 105, 19335-19351.

996 Polteau, S., Ferré, E.C., Planke, S., Neumann, E.R., Chevallier, L., 2008. How are saucer-
997 shaped sills emplaced? Constraints from the Golden Valley Sill, South Africa. *Journal of*
998 *Geophysical Research: Solid Earth* 113.

999 Price, R., Chappell, B., 1975. Fractional crystallisation and the petrology of Dunedin
1000 Volcano. *Contributions to mineralogy and petrology* 53, 157-182.

1001 Pryer, L., Weir, J., Debacker, T., Romine, K., 2013. Interpretation of basement: NZ ECS
1002 SEEBASE: Advantage New Zealand Petroleum Summit. April.

- 1003 Quirie, A.K., Schofield, N., Hartley, A., Hole, M.J., Archer, S.G., Underhill, J.R., Watson,
1004 D., Holford, S.P., 2019. The Rattray Volcanics: Mid-Jurassic fissure volcanism in the UK
1005 Central North Sea. *Journal of the Geological Society* 176, 462-481.
- 1006 Rawlinson, N., Davies, D.R., Pilia, S., 2017. The mechanisms underpinning Cenozoic
1007 intraplate volcanism in eastern Australia: Insights from seismic tomography and geodynamic
1008 modeling. *Geophysical Research Letters* 44, 9681-9690.
- 1009 Reeves, J., Magee, C., Jackson, C., 2018. Unravelling intrusion-induced forced fold
1010 kinematics and ground deformation using 3D seismic reflection data. *Volcanica*, 1-17.
- 1011 Reynolds, P., Holford, S., Schofield, N., Ross, A., 2017. Three-Dimensional Seismic Imaging
1012 of Ancient Submarine Lava Flows: An Example From the Southern Australian Margin.
1013 *Geochemistry, Geophysics, Geosystems* 18, 3840-3853.
- 1014 Reynolds, P., Schofield, N., Brown, R.J., Holford, S.P., 2018. The architecture of submarine
1015 monogenetic volcanoes – insights from 3D seismic data. *Basin Res* 30, 437-451.
- 1016 Robertson, A.H.F., Campbell, H.J., Johnston, M.R., Palamakumbra, R., 2019. Chapter 15
1017 Construction of a Paleozoic–Mesozoic accretionary orogen along the active continental
1018 margin of SE Gondwana (South Island, New Zealand): summary and overview. *Geological*
1019 *Society, London, Memoirs* 49, 331-372.
- 1020 Rout, D.J., Cassidy, J., Locke, C.A., Smith, I.E.M., 1993. Geophysical evidence for temporal
1021 and structural relationships within the monogenetic basalt volcanoes of the Auckland
1022 volcanic field, northern New Zealand. *Journal of Volcanology and Geothermal Research* 57,
1023 71-83.
- 1024 Sahoo, T., King, P., Bland, K., Strogen, D., Sykes, R., Bache, F., 2014. Tectono-sedimentary
1025 evolution and source rock distribution of the mid to Late Cretaceous succession in the Great
1026 South Basin, New Zealand *The APPEA Journal* 54, 259-274.
- 1027 Schofield, N., Holford, S., Millett, J., Brown, D., Jolley, D., Passey, S.R., Muirhead, D.,
1028 Grove, C., Magee, C., Murray, J. and Hole, M., 2017. Regional magma plumbing and
1029 emplacement mechanisms of the Faroe-Shetland Sill Complex: implications for magma
1030 transport and petroleum systems within sedimentary basins. *Basin Research*, 29(1), pp.41-63.
- 1031 Slatt, R.M., 2006. Stratigraphic reservoir characterization for petroleum geologists,
1032 geophysicists, and engineers. Elsevier.
- 1033 Sleep, N.H., 1992. Hotspot volcanism and mantle plumes. *Annual Review of Earth and*
1034 *Planetary Sciences* 20, 19-43.
- 1035 Smallwood, J.R., Maresh, J., 2002. The properties, morphology and distribution of igneous
1036 sills: modelling, borehole data and 3D seismic from the Faroe-Shetland area. *Geological*
1037 *Society, London, Special Publications* 197, 271.

- 1038 Speight, R., 1943. The geology of Banks Peninsula: a revision, Transactions of the New
1039 Zealand Institute, pp. 13-26.
- 1040 Spörli, K.B., Black, P.M., Lindsay, J.M., 2015. Excavation of buried Dun Mountain–Maitai
1041 terrane ophiolite by volcanoes of the Auckland Volcanic field, New Zealand. New Zealand
1042 Journal of Geology and Geophysics 58, 229-243.
- 1043 Spörli, K.B., Eastwood, V.R., 1997. Elliptical boundary of an intraplate volcanic field,
1044 Auckland, New Zealand. Journal of Volcanology and Geothermal Research 79, 169-179.
- 1045 Stephens, T.L., Walker, R.J., Healy, D., Bubeck, A., England, R.W., McCaffrey, K.J.W.,
1046 2017. Igneous sills record far-field and near-field stress interactions during volcano
1047 construction: Isle of Mull, Scotland. Earth and Planetary Science Letters 478, 159-174.
- 1048 Stipp, J.J., McDougall, I., 1968. Geochronology of the Banks Peninsula Volcanoes, New
1049 Zealand. New Zealand Journal of Geology and Geophysics 11, 1239-1258.
- 1050 Sun, Q., Jackson, C.A.L., Magee, C., Mitchell, S.J., Xie, X., 2019a. Extrusion dynamics of
1051 deep-water volcanoes. Solid Earth Discuss. 2019, 1-40.
- 1052 Sun, Q., Jackson, C.A., Magee, C. and Xie, X., 2020. Deeply buried ancient volcanoes
1053 control hydrocarbon migration in the South China Sea. *Basin Research*, 32(1), pp.146-162
- 1054 Sutherland, R., 1995. The Australia-Pacific boundary and Cenozoic plate motions in the SW
1055 Pacific: Some constraints from Geosat data. Tectonics 14, 819-831.
- 1056 Sutherland, R., 1999. Basement geology and tectonic development of the greater New
1057 Zealand region: an interpretation from regional magnetic data. Tectonophysics 308, 341-362.
- 1058 Symonds, P.A., Planke, S., Frey, O., Skogseid, J., 1998. Volcanic evolution of the Western
1059 Australian continental margin and its implications for basin development.
- 1060 Tarling, M.S., Smith, S.A.F., Scott, J.M., Rooney, J.S., Viti, C., Gordon, K.C., 2019. The
1061 internal structure and composition of a plate-boundary-scale serpentinite shear zone: the
1062 Livingstone Fault, New Zealand. Solid Earth 10, 1025-1047.
- 1063 Thomson, K., 2005. Volcanic features of the North Rockall Trough: application of
1064 visualisation techniques on 3D seismic reflection data. Bulletin of Volcanology 67, 116-128.
- 1065 Thomson, K., Hutton, D., 2004. Geometry and growth of sill complexes: insights using 3D
1066 seismic from the North Rockall Trough. Bulletin of Volcanology 66, 364-375.
- 1067 Timm, C., Hoernle, K., Van Den Bogaard, P., Bindeman, I., Weaver, S., 2009. Geochemical
1068 Evolution of Intraplate Volcanism at Banks Peninsula, New Zealand: Interaction Between
1069 Asthenospheric and Lithospheric Melts. Journal of Petrology 50, 989-1023.

- 1070 Timm, C., Hoernle, K., Werner, R., Hauff, F., den Bogaard, P.v., White, J., Mortimer, N.,
1071 Garbe-Schönberg, D., 2010. Temporal and geochemical evolution of the Cenozoic intraplate
1072 volcanism of Zealandia. *Earth-Science Reviews* 98, 38-64.
- 1073 Trude, J., Cartwright, J., Davies, R.J., Smallwood, J., 2003. New technique for dating igneous
1074 sills. *Geology* 31, 813-816.
- 1075 Tulloch, A., Mortimer, N., Ireland, T., Waight, T., Maas, R., Palin, M., Sahoo, T., Seebeck,
1076 H., Sagar, M., Barrier, A., Turnbull, R., 2019. Reconnaissance basement geology and
1077 tectonics of South Zealandia. *Tectonics* 0.
- 1078 Uruski, C., 2015. The contribution of offshore seismic data to understanding the evolution of
1079 the New Zealand continent. *Geol Soc Spec Publ* 413, 35-51.
- 1080 Uruski, C., Kennedy, C., Harrison, T., Maslen, G., Cook, R., Sutherland, R., Zhu, H., 2007.
1081 Petroleum potential of the Great South Basin, New Zealand—New seismic data improves
1082 imaging. *The APPEA Journal* 47, 145-161.
- 1083 Uruski, C.I., 2010. New Zealand's deepwater frontier. *Marine and Petroleum Geology* 27,
1084 2005-2026.
- 1085 Valentine, G.A., Hirano, N., 2010. Mechanisms of low-flux intraplate volcanic fields—Basin
1086 and Range (North America) and northwest Pacific Ocean. *Geology* 38, 55-58.
- 1087 Waight, T.E., Weaver, S.D., Maas, R., Eby, G.N., 1998. French Creek Granite and Hohonu
1088 Dyke Swarm, South Island, New Zealand: Late Cretaceous alkaline magmatism and the
1089 opening of the Tasman Sea. *Australian Journal of Earth Sciences* 45, 823-835.
- 1090 Walker, F., Schofield, N., Millett, J., Jolley, D., Hole, M., Stewart, M., 2019. Paleogene
1091 volcanic rocks in the northern Faroe-Shetland Basin and Møre Marginal High: Understanding
1092 lava field stratigraphy. *Geological Society, London, Special Publications* 495, SP495-2019-
1093 2013.
- 1094 Wall, M., Cartwright, J., Davies, R., McGrandle, A., 2010. 3D seismic imaging of a Tertiary
1095 Dyke Swarm in the Southern North Sea, UK. *Basin Res* 22, 181-194.
- 1096 Widess, M.B., 1973. How thin is a thin bed? *Geophysics* 38, 1176-1180.
- 1097 Wilson, C., Houghton, B., McWilliams, M., Lanphere, M., Weaver, S., Briggs, R., 1995.
1098 Volcanic and structural evolution of Taupo Volcanic Zone, New Zealand: a review. *Journal*
1099 *of volcanology and geothermal research* 68, 1-28.
- 1100 Woodward, D., Hatherton, T., 1975. Magnetic anomalies over southern New Zealand. *New*
1101 *Zealand journal of geology and geophysics* 18, 65-82.

Wright, K.A., Davies, R.J., Jerram, D.A., Morris, J., Fletcher, R., 2012. Application of seismic and sequence stratigraphic concepts to a lava-fed delta system in the Faroe-Shetland Basin, UK and Faroes. *Basin Res* 24, 91-106.

Wright, N.M., Seton, M., Williams, S.E., Müller, R.D., 2016. The Late Cretaceous to recent tectonic history of the Pacific Ocean basin. *Earth-Science Reviews* 154, 138-173.

Wu, L., Mei, L., Paton, D.A., Guo, P., Liu, Y., Luo, J., Wang, D., Li, M., Zhang, P., Wen, H., 2018. Deciphering the origin of the Cenozoic intracontinental rifting and volcanism in eastern China using integrated evidence from the Jiangnan Basin. *Gondwana Research* 64, 67-83.

Zhao, F., Wu, S., Sun, Q., Huuse, M., Li, W., Wang, Z., 2014. Submarine volcanic mounds in the Pearl River Mouth Basin, northern South China Sea. *Marine Geology* 355, 162-172.

Figure Captions

Figure 1 – A) Onshore relief and offshore bathymetry map of the South Island of New Zealand highlighting the location of the Tuatara Volcanic Field and selected further intraplate volcanic products across the South Island. Also shown are the locations of the major terrane boundaries across the area (after Mortimer et al 2002). Inset – Map showing the regional basement geology across New Zealand. B) Tectono-stratigraphic column showing the major stratigraphy present in the Great South Basin, as well as the timings of regional tectonics and volcanism. After Bertoni et al. (2019); Higgs et al. (2019); Mortimer et al. (2014).

Figure 2 – A) Magnetic anomaly map across the northern part of the Great South Basin. Data are reduced to pole in order to place the anomalies vertically above the magnetic source. The locations of major magnetic anomalies are shown after Tulloch et al. (2019) and Sutherland et al. (1999). The magnetic data are courtesy of the NZ SEEBASE database (Pryer et al., 2013). B) Two-way-time structure map of the top surface of the central edifice of the Tuatara Volcanic Field. The locations of prominent volcanic cones are shown by the white triangles. See Figure 1 for location.

Figure 3 – Uninterpreted and interpreted NW-SE oriented seismic section across the Tuatara Volcanic Field. The central edifice of the field is identified as a package of high-amplitude reflectivity, with

1131 igneous sills and volcanic cones identified around the main structure. Image quality is greatly reduced
1132 beneath the main edifice. See Figure 2 for location.

1133 Figure 4 – Uninterpreted and interpreted NE-SW oriented seismic section across the Tuatara Volcanic
1134 Field. The central edifice (shown in grey) is surrounded by multiple volcanic cones and igneous sills.
1135 Image quality is greatly reduced beneath the central edifice. See Figure 2 for location.

1136 Figure 5 – Close-up seismic sections and interpretations of the tabular lava sequences that comprise
1137 the central edifice of the Tuatara Volcanic Field. Stacked lava sequences, individual volcanic cones
1138 and lava delta sequences are highlighted in the interpretations. See Figure 2 for location.

1139 Figure 6 – Interpreted seismic sections highlighting the morphology and seismic expression of
1140 volcanic cones within the Tuatara Volcanic Field. See Figure 7 for the locations of individual
1141 sections.

1142 Figure 7 – A) Map showing the age and distribution of interpreted volcanic cones surrounding the
1143 Tuatara Volcanic Field. B) Map showing the age of emplacement and distribution of igneous sills
1144 within and surrounding the Tuatara Volcanic Field. Note that the igneous sills are more widely
1145 distributed around the central edifice compared to the volcanic cones.

1146 Figure 8 – Uninterpreted and interpreted seismic section showing a minor volcanic cone to the south
1147 of the main edifice. See Figure 2 for location. Note the presence of Early Eocene aged lava flows
1148 associated with the volcanic cone.

1149 Figure 9 – Interpreted seismic sections showing a number of different sills interpreted throughout the
1150 area. See Figure 7 for location. The age of sill emplacement can be estimated as the age of the strata
1151 onlapping onto the identified forced folds.

1152 Figure 10 – A) Schematic cartoon showing the overall evolution of the Tuatara Volcanic Field. Sill
1153 emplacement and volcanism begins in the Late Cretaceous, with the majority of activity, including the
1154 formation of the majority of the central edifice occurring in the Paleocene. Activity migrates towards
1155 the northwest and wanes throughout the early Eocene, before the Tuatara Field becomes buried. B)

Map showing the distribution of sills and volcanic cones within the Tuatara Volcanic Field. The distribution of volcano-magmatic features is co-located with the Livingstone Fault, forming the boundary between the Caples and Dun Mountain-Maitai Terranes. Inset – Cartoon showing the setting of the Auckland Volcanic Field, located between the same basement terranes on the North Island of New Zealand. C) Regional model for the localisation of activity in the Tuatara Volcanic Field. Upper crustal basement terranes are based on the SESI seismic section along the east coast of the South Island of New, after Mortimer et al. (2002). The lower part of the figure shows the hypothesised model for lithosphere detachment and melt generation in the lithosphere. See Figure 1 for location of SESI seismic section.

Figure 11 – 3D block model showing the geometry of the Tuatara Volcanic Field and its hypothesised link to magma generation at the base of the lithosphere. Areas of detaching material from the base of the lithosphere promote decompression melting of upwelling asthenosphere. The detachment of lithospheric material progressively migrates northwest-wards along the Livingstone Fault terrane boundary, causing the age progression identified in the Tuatara Volcanic Field. The field is thought to be dominated by vertical magma transport throughout the lithosphere, and is dominated by sills in the upper crust.

Supplementary Figure 1 – Interpreted seismic section linking the study area to the nearby Toroa-1 borehole, providing age constraints on the shallow sedimentary succession of the Tuatara Volcanic Field. Although located a great distance from the study area, the intervening geology between the borehole and the Tuatara Volcanic Field is relatively simple, dominated by post-rift strata allowing us to correlate horizons across the study area. See Figure 2 for location.

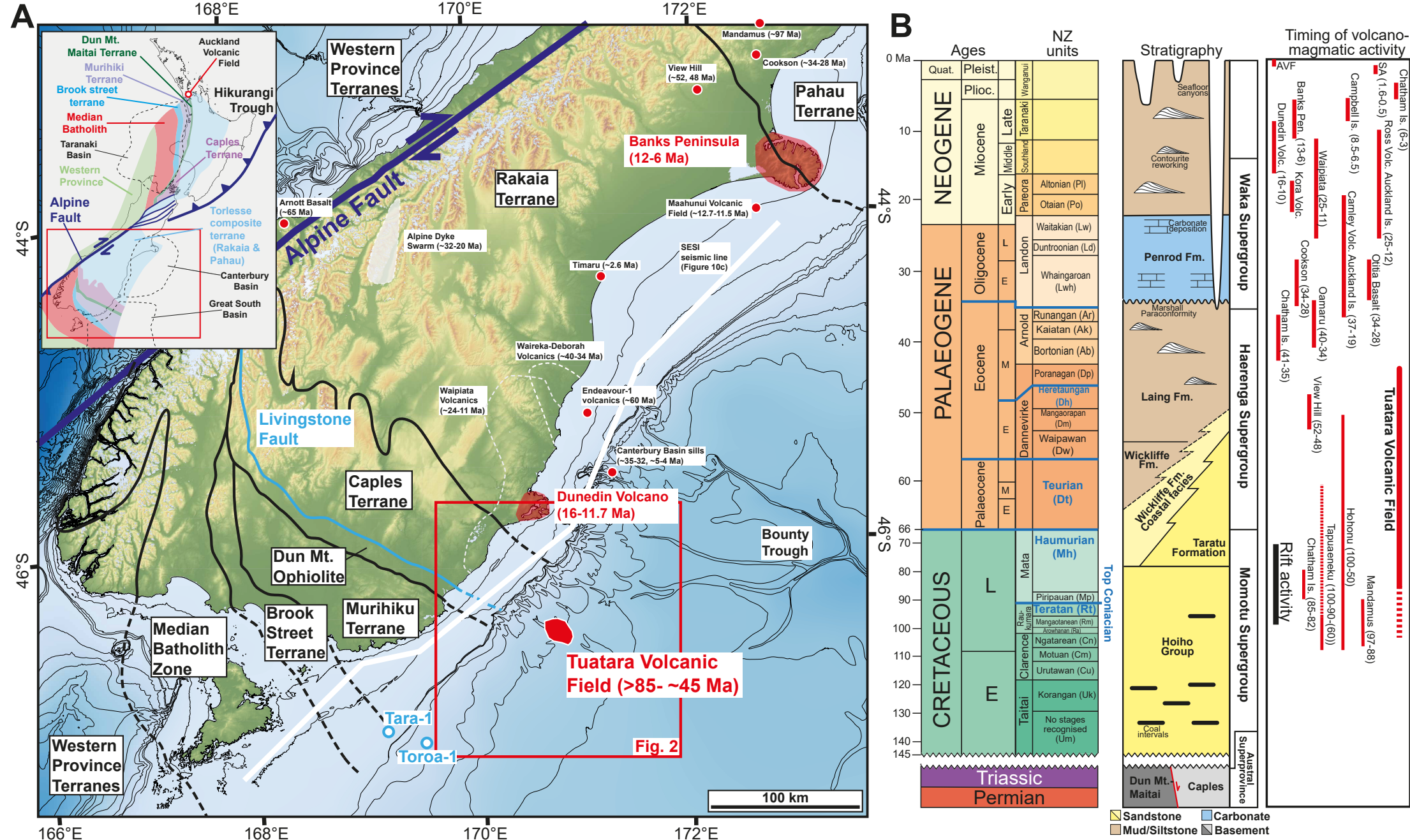


Figure 1

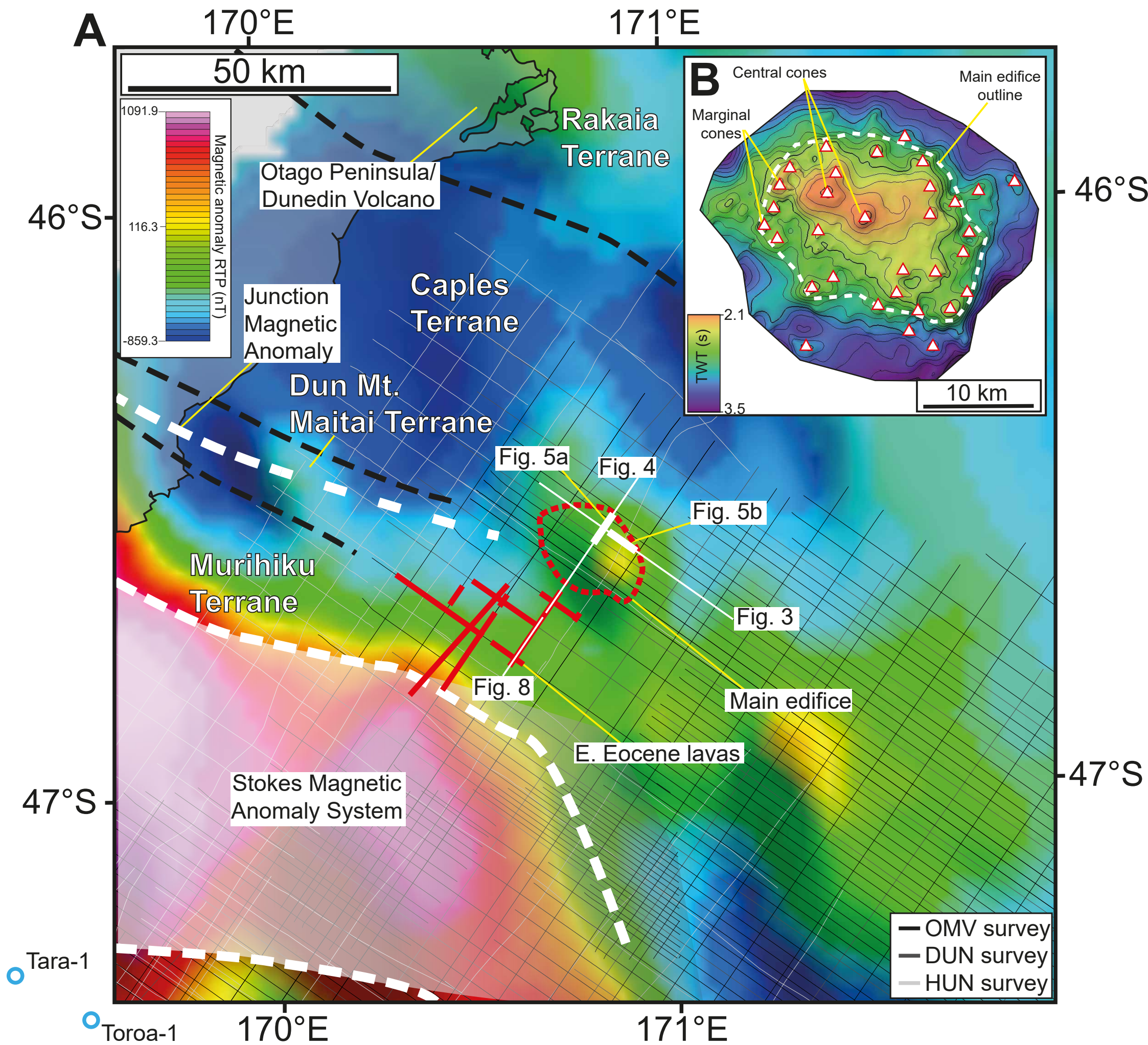


Figure 2

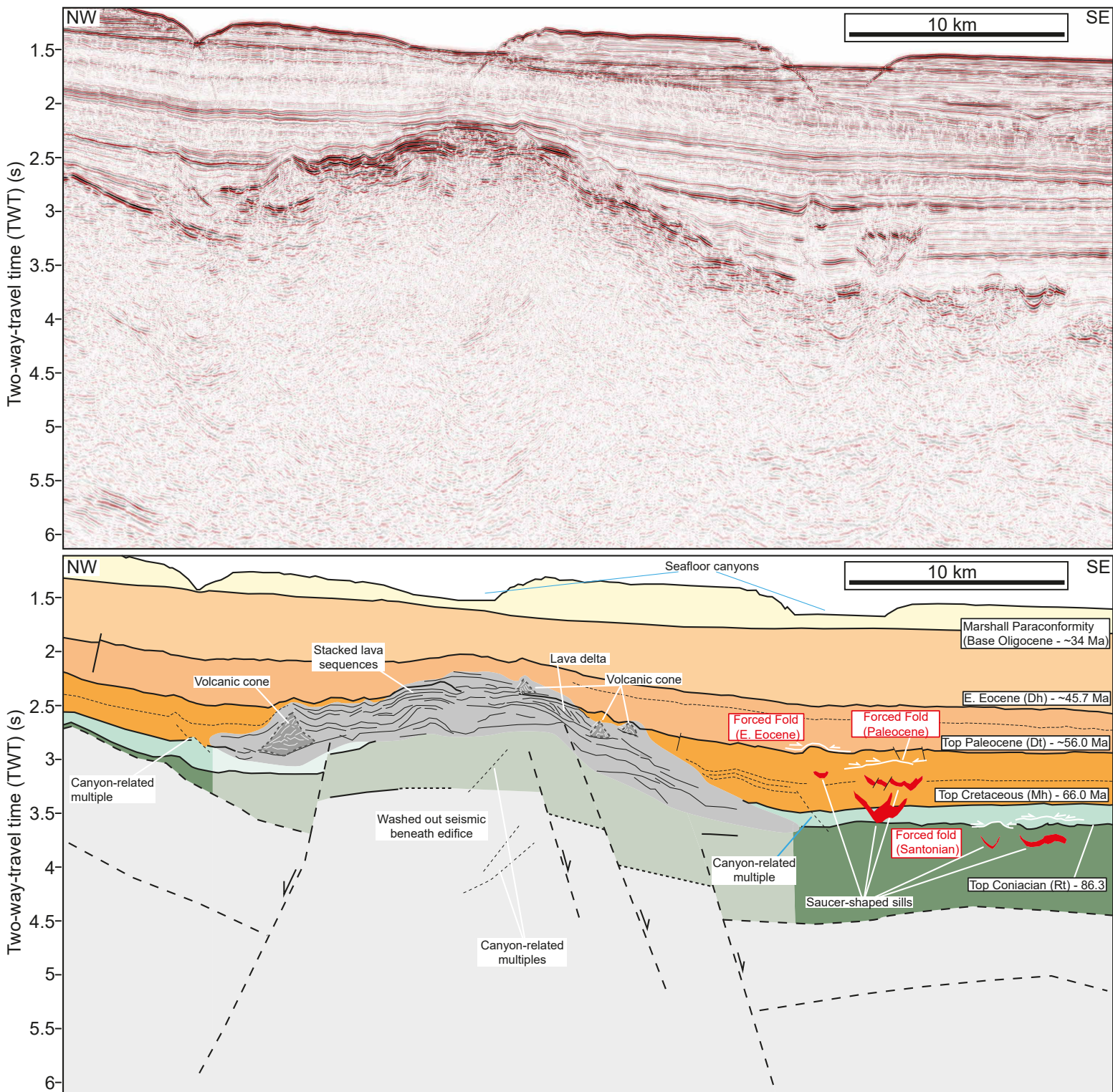


Figure 3

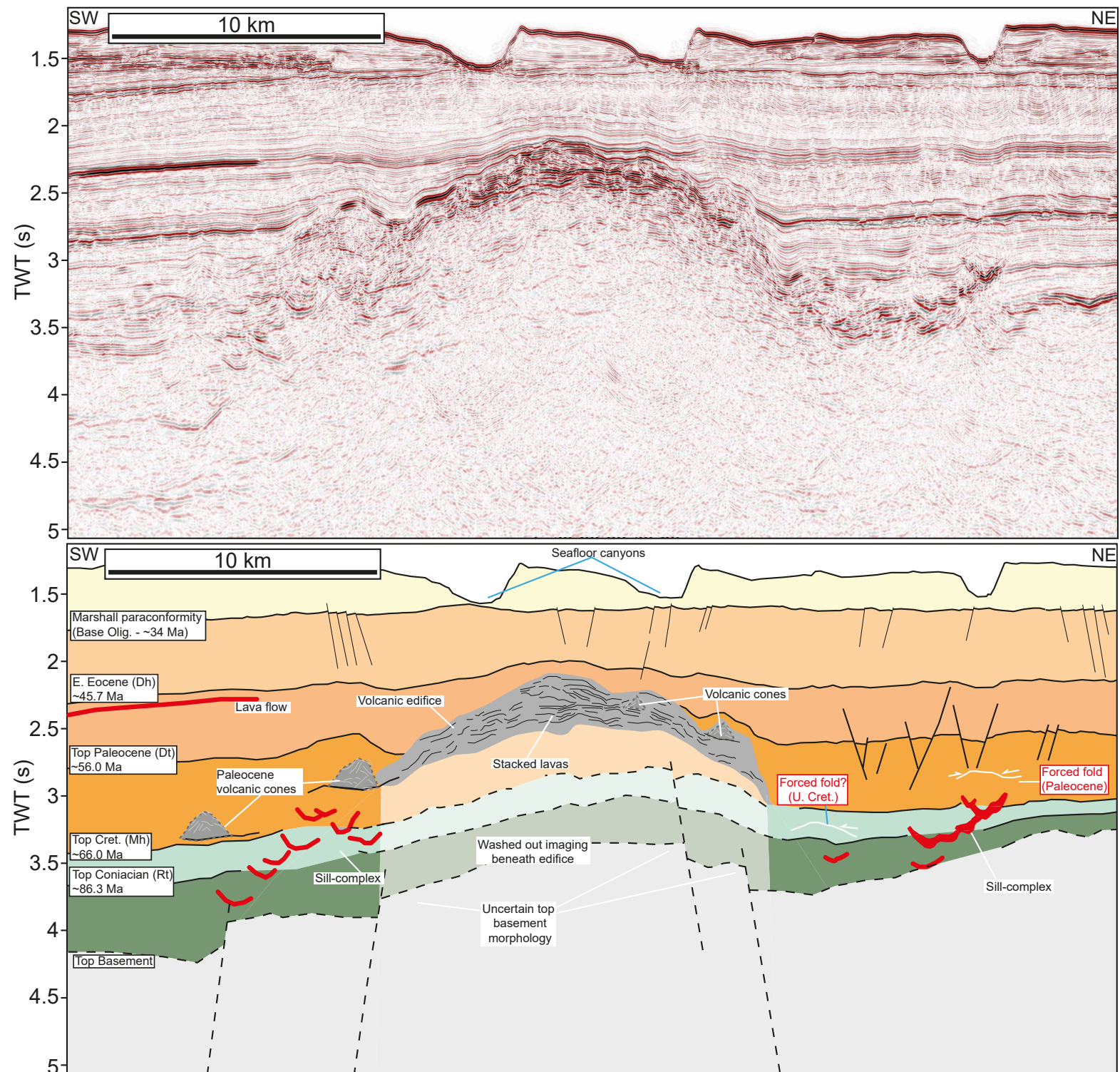


Figure 4

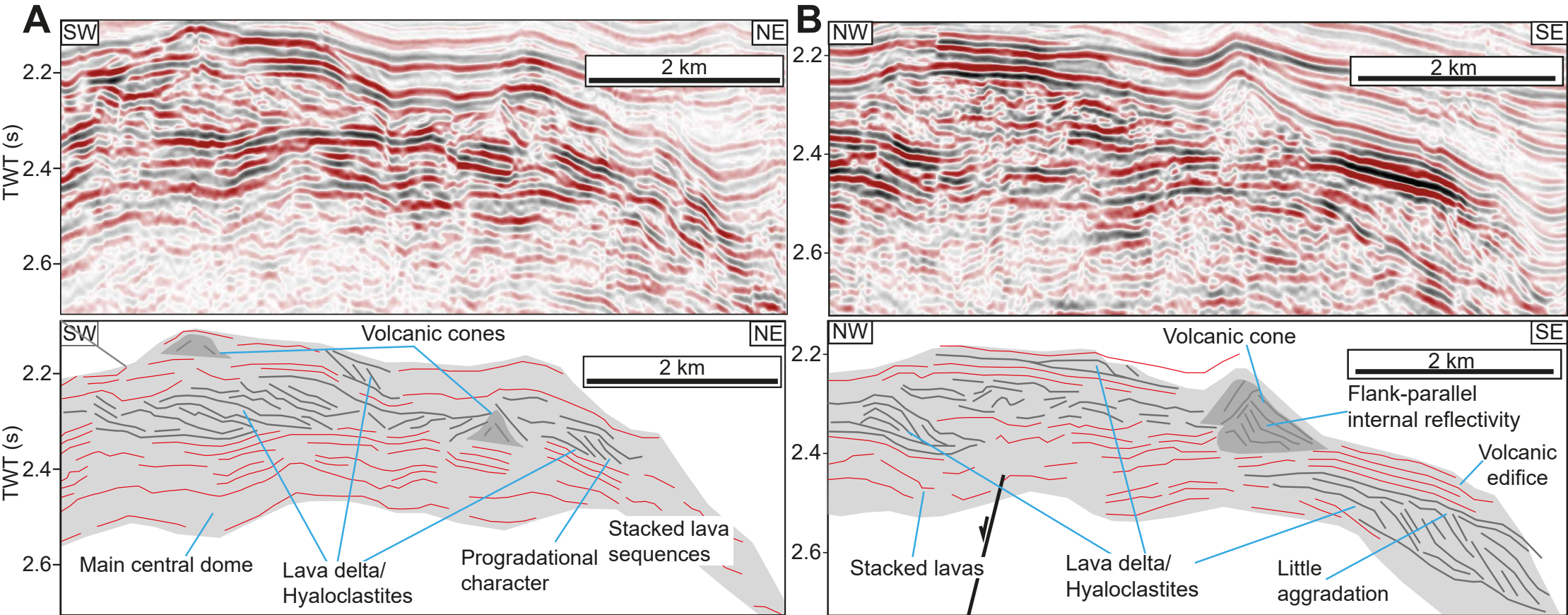


Figure 5

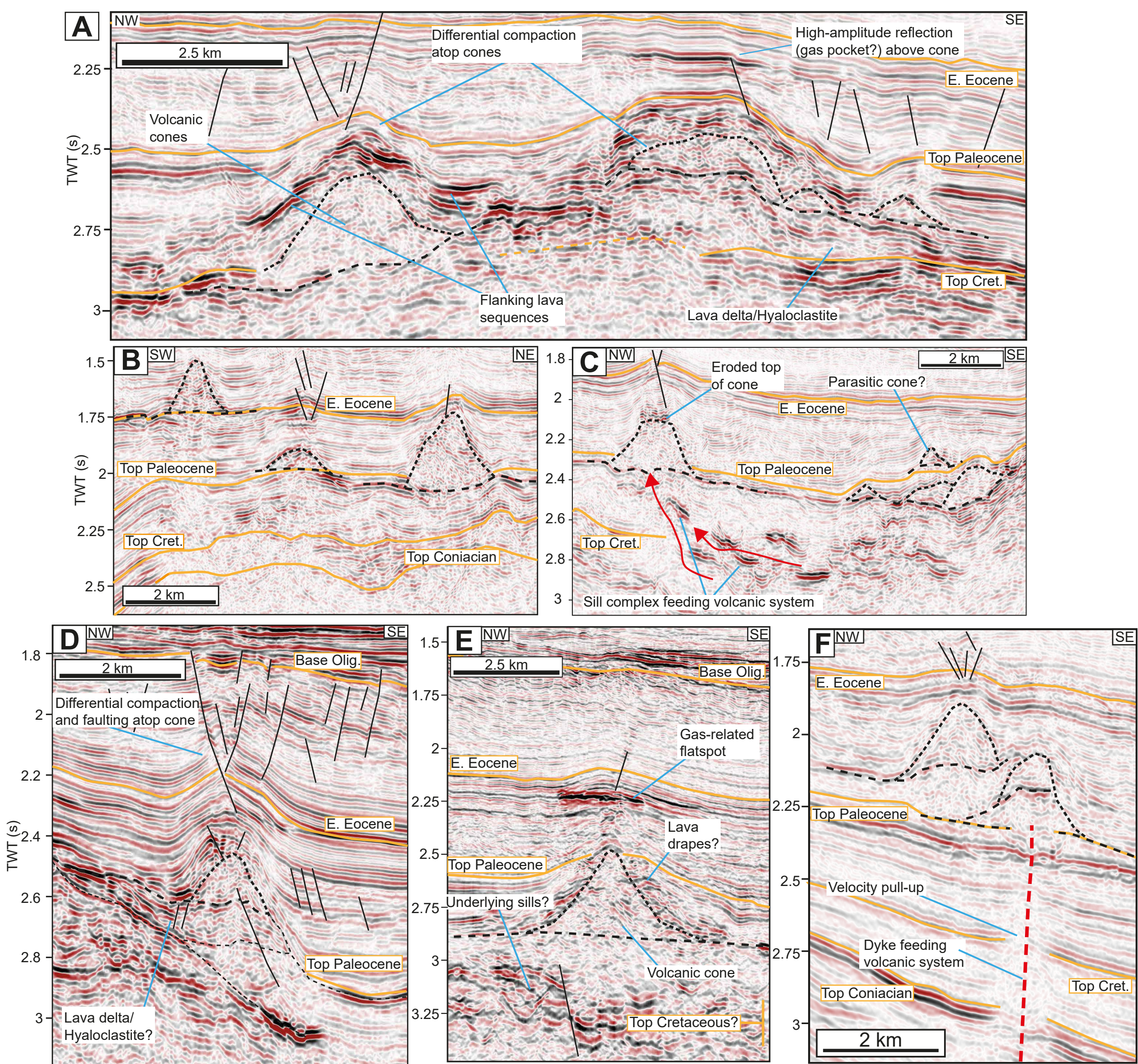


Figure 6

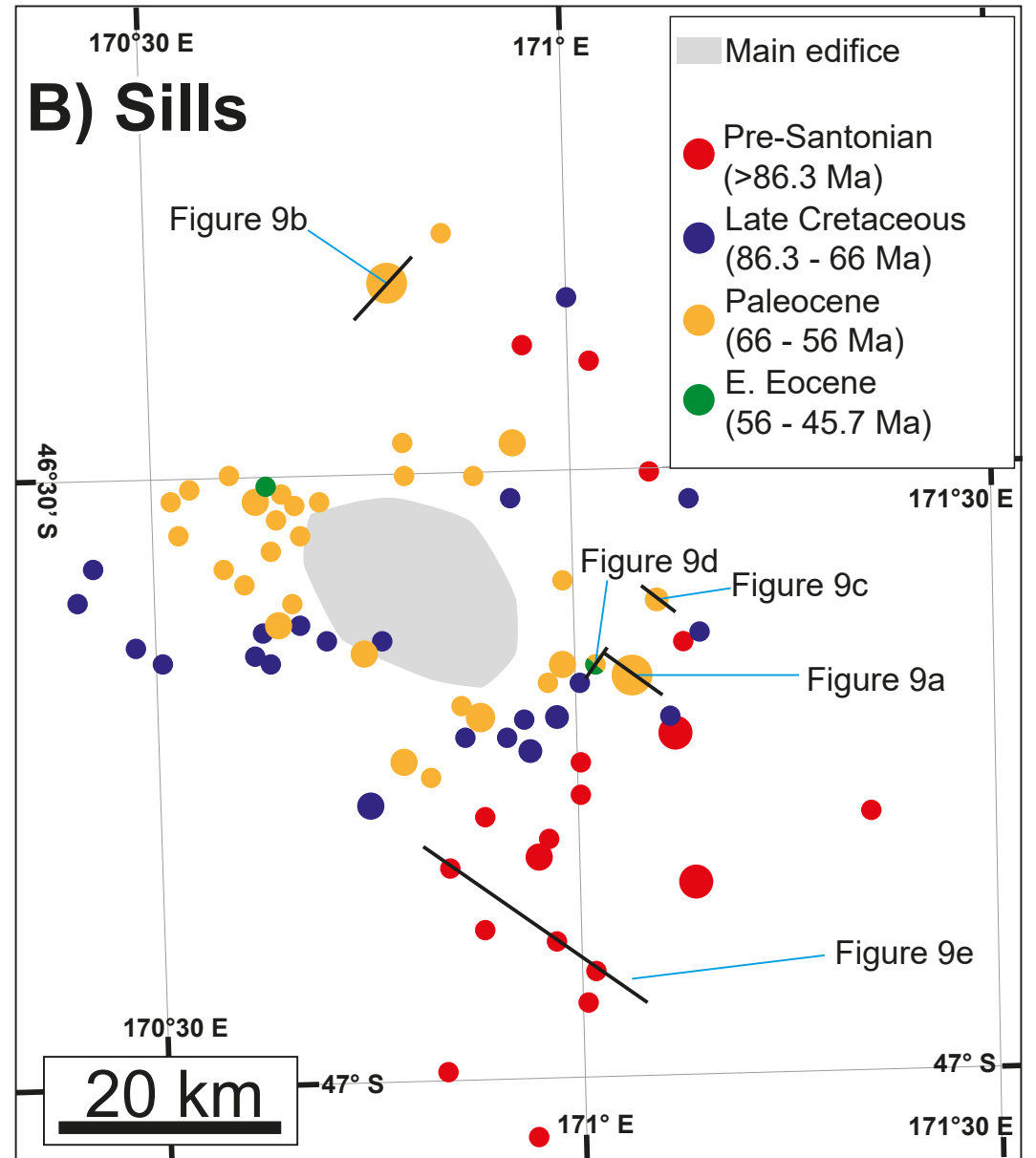
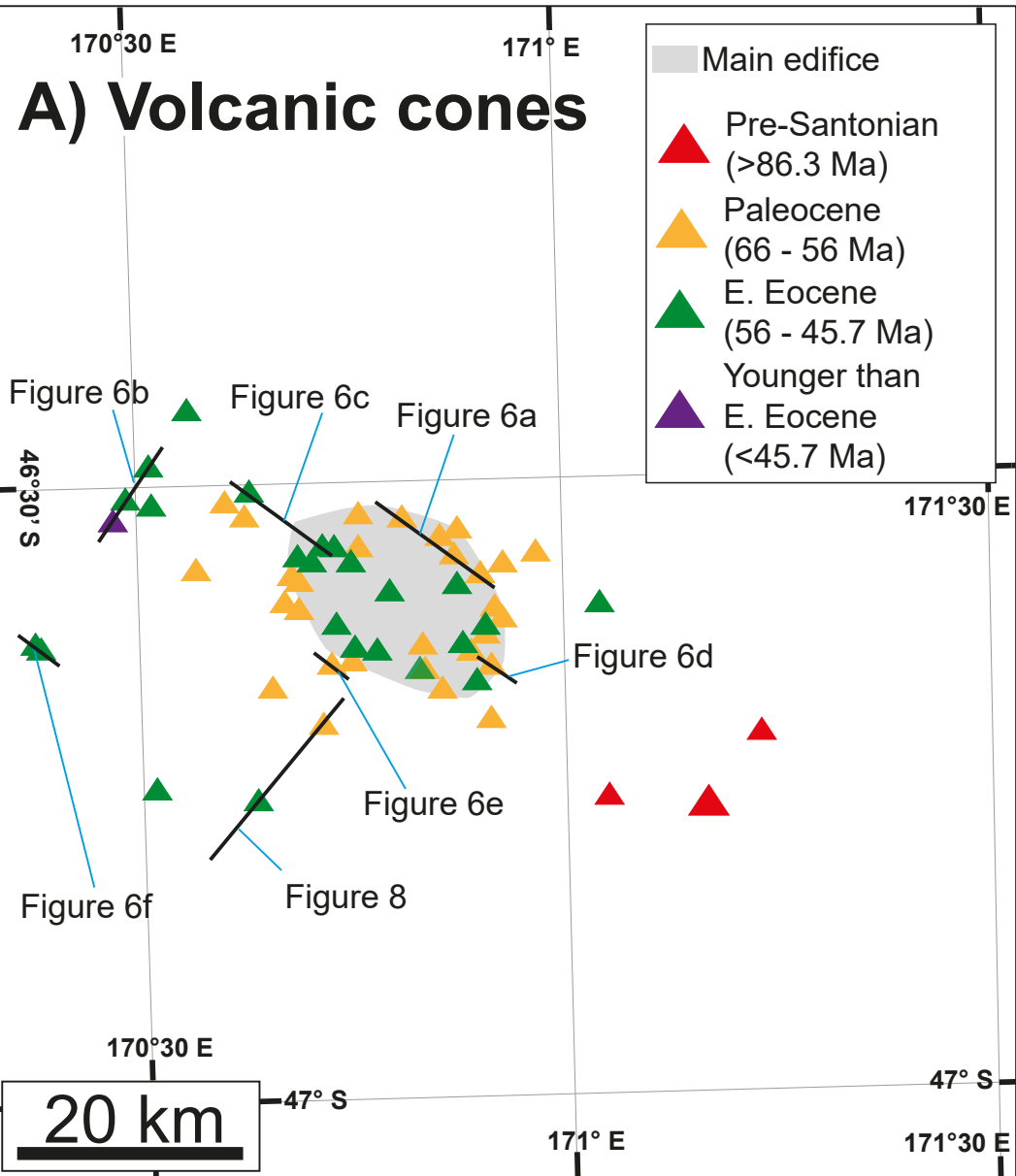


Figure 7

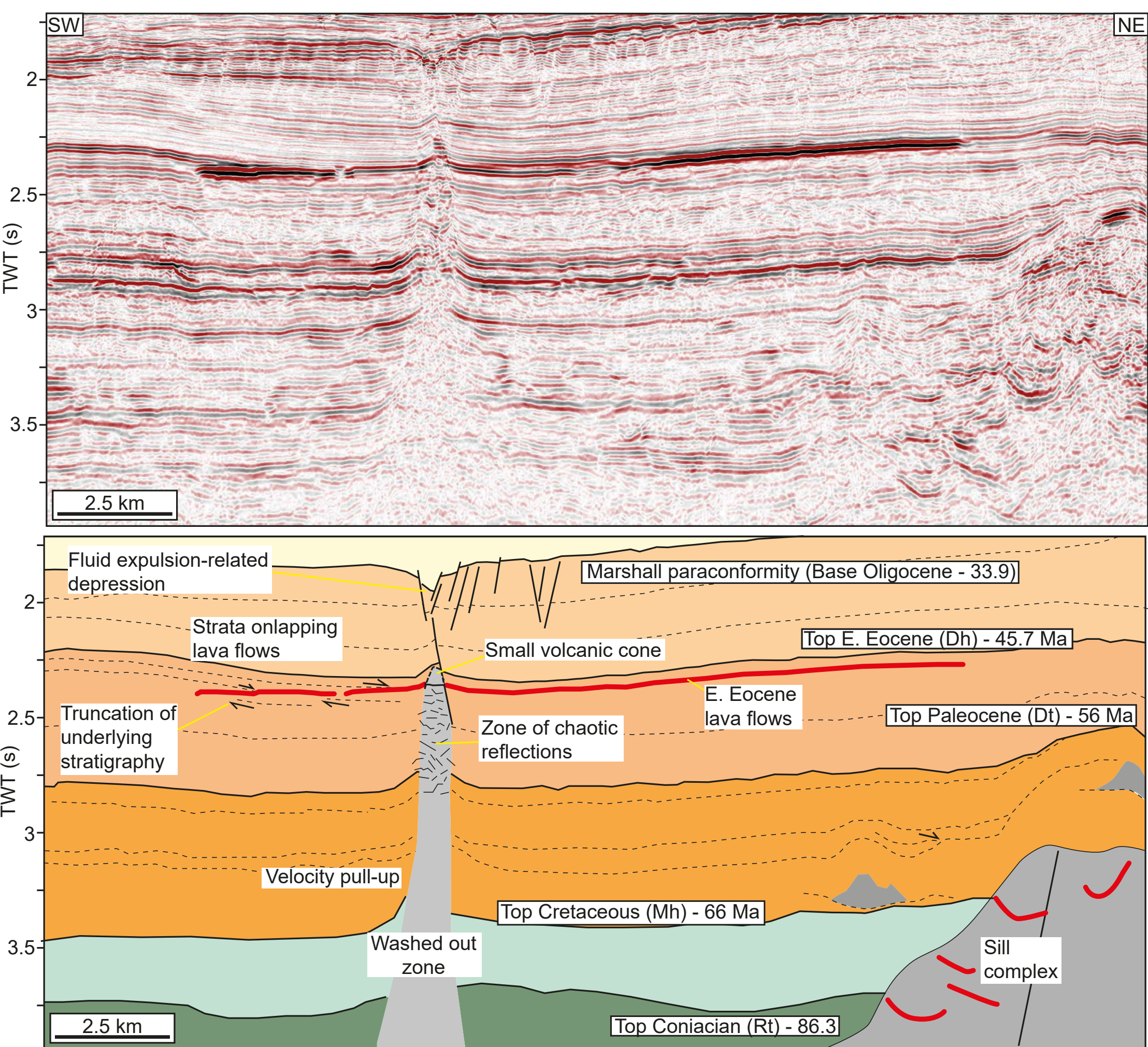


Figure 8

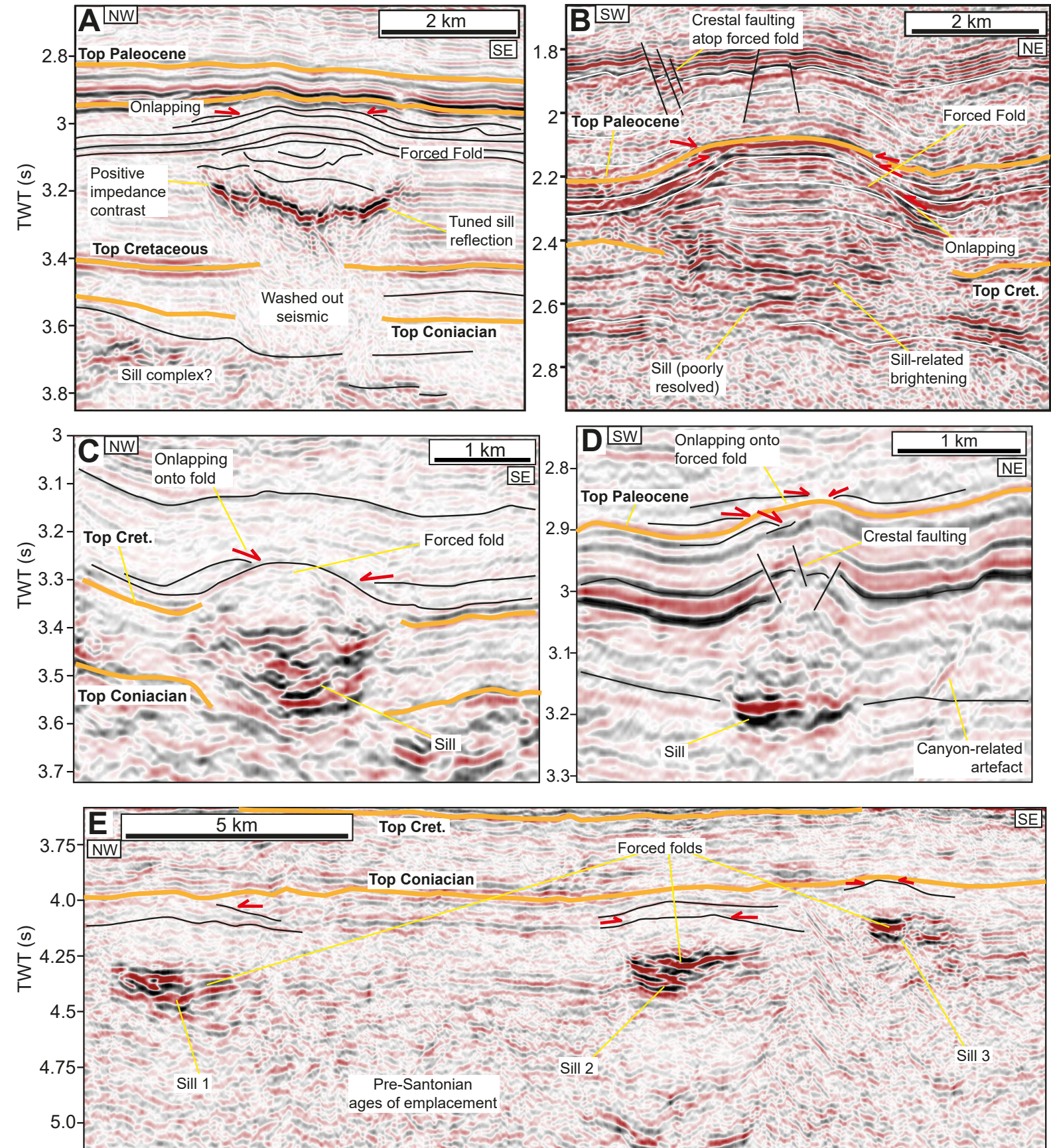


Figure 9

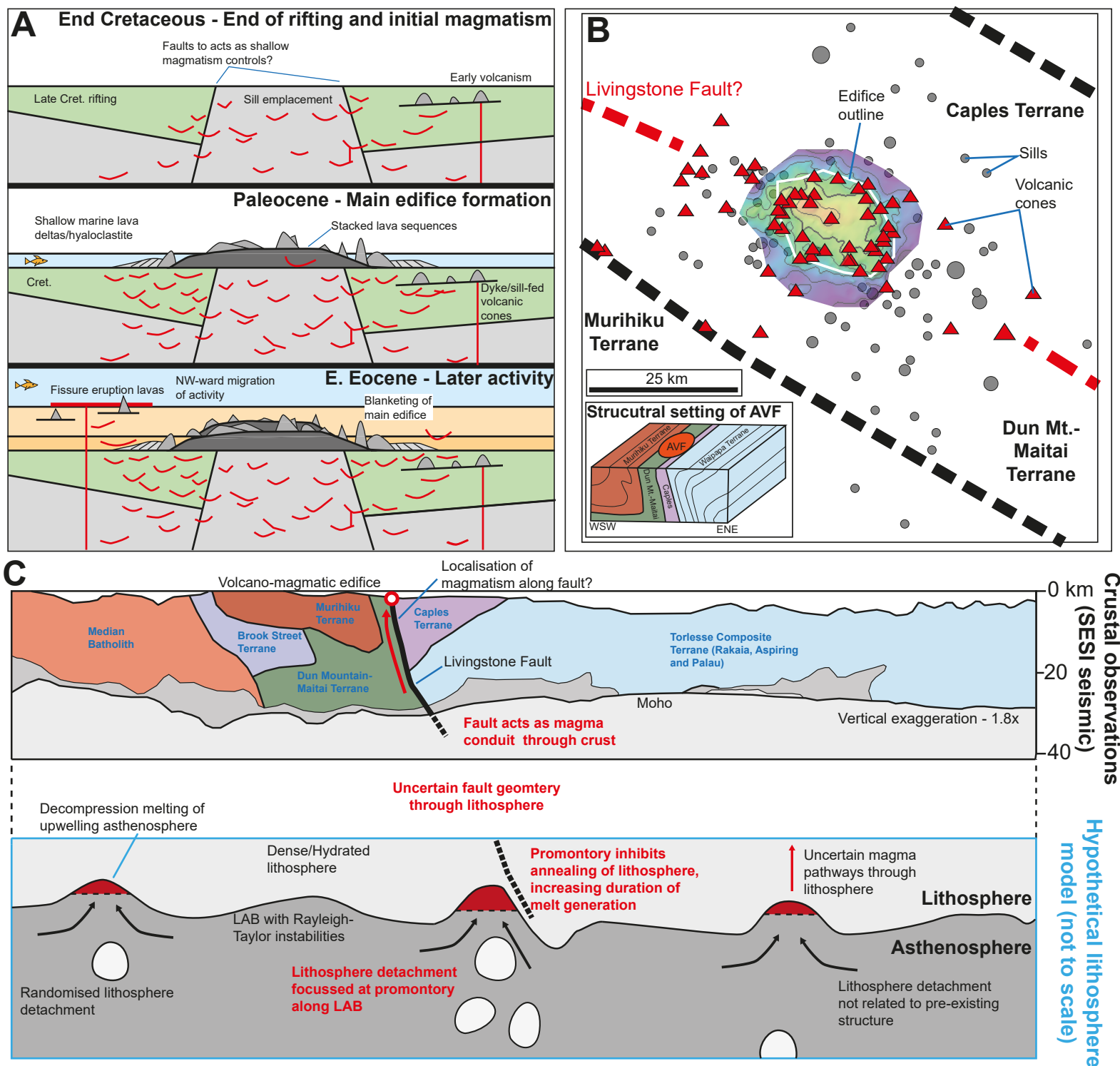


Figure 10

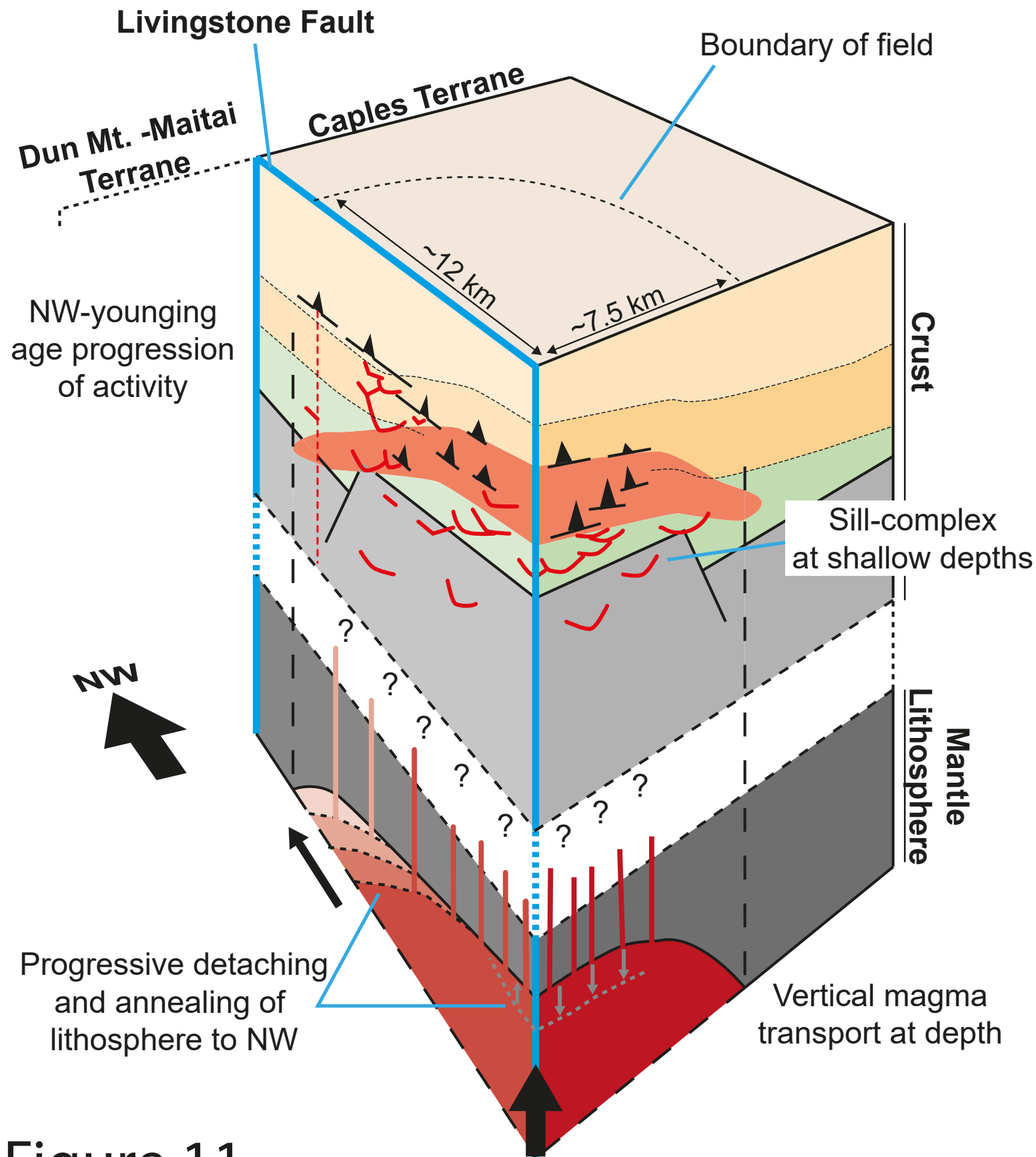
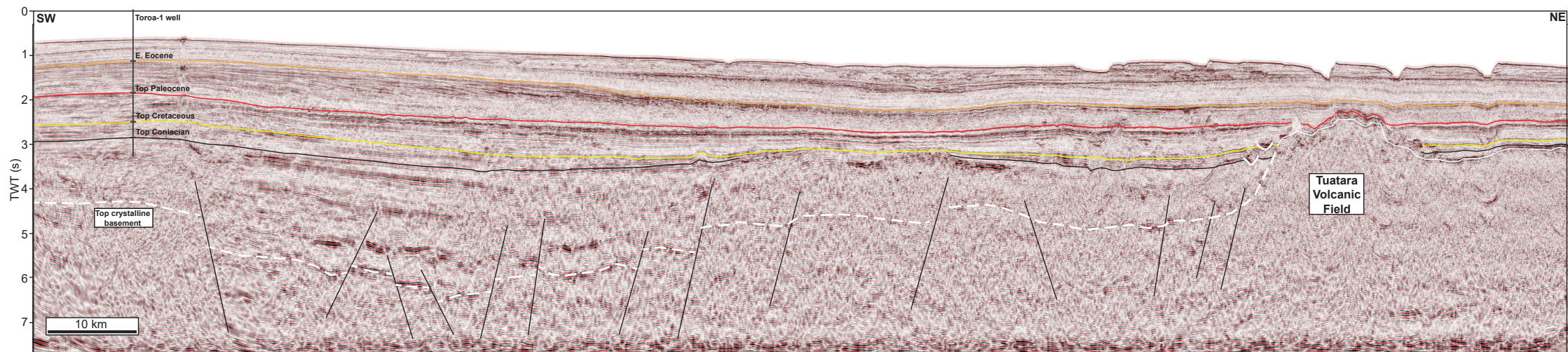


Figure 11



Supplementary Figure 1